Chemical Geology 253 (2008) 180–195

Contents lists available at ScienceDirect

Chemical Geology

journal homepage: www.elsevier.com/locate/chemgeo

He–Ar and Nd–Sr isotopic compositions of late Pleistocene felsic plutonic back arc basin rocks from Ulleungdo volcanic island, South Korea: Implications for the genesis of young plutonic rocks in a back arc basin

Kyu Han Kim [a,*], Keisuke Nagao [b], Hirochika Sumino [b], Tsuyoshi Tanaka [c], Takamasa Hayashi [c], Toshio Nakamura [d], Jong Ik Lee [e]

[a] Department of Science Education, Ewha Womans University, Seoul 120-750, South Korea
[b] Laboratory for Earthquake Chemistry, Graduate School of Science, University of Tokyo, Tokyo 113-0033, Japan
[c] Department of Earth and Environmental Sciences, Nagoya University, Nagoya 464-8602, Japan
[d] Center for Chronological Research, Nagoya University, Nagoya 464-8602, Japan
[e] Korea Polar Research Institute, KORDI, Songdo Techno Park, Incheon 406-840, South Korea

ARTICLE INFO

Article history:
Received 20 March 2007
Received in revised form 4 April 2008
Accepted 13 May 2008

Editor: R.L. Rudnick

Keywords:
Mantle helium
Excess argon
Nd–Sr isotopes
Felsic plutonic rocks
Alkali basaltic magma
Ulleungdo volcanic island

ABSTRACT

We report analyses of noble gases and Nd–Sr isotopes in mineral separates and whole rocks of late Pleistocene (<0.2 Ma) monzonites from Ulleungdo, South Korea, a volcanic island within the back arc basin of the Japan island arc. A Rb–Sr mineral isochron age for the monzonites is 0.12±0.01 Ma. K–Ar biotite ages from the same samples gave relatively concordant ages of 0.19±0.01and 0.22±0.01 Ma. $^{40}Ar/^{39}Ar$ yields a similar age of 0.29±0.09 Ma. Geochemical characteristics of the felsic plutonic rocks, which are silica oversaturated alkali felsic rocks (av., 12.5 wt% in K_2O+Na_2O), are similar to those of 30 alkali volcanics from Ulleungdo in terms of concentrations of major, trace and REE elements. The initial Nd–Sr isotopic ratios of the monzonites ($^{87}Sr/^{86}Sr=0.70454–0.71264$, $^{143}Nd/^{144}Nd=0.512528–0.512577$) are comparable with those of the alkali volcanics ($^{87}Sr/^{86}Sr=0.70466–0.70892$, $^{143}Nd/^{144}Nd=0.512521–0.512615$) erupted in Stage 3 of Ulleungdo volcanism (0.24–0.47 Ma). The high initial $^{87}Sr/^{86}Sr$ values of the monzonites imply that seawater and crustally contaminated pre-existing trachytes may have been melted or assimilated during differentiation of the alkali basaltic magma.

A mantle helium component ($^3He/^4He$ ratio of up to 6.5 RA) associated with excess argon was found in the monzonites. Feldspar and biotite have preferentially lost helium during slow cooling at depth and/or during their transportation to the surface in a hot host magma. The source magma noble gas isotopic features are well preserved in fluid inclusions in hornblende, and indicate that the magma may be directly derived from subcontinental lithospheric mantle metasomatized by an ancient subduction process, or may have formed as a mixture of MORB-like mantle and crustal components. The radiometric ages, geochemical and Nd–Sr isotopic signatures of the Ulleungdo monzonites as well as the presence of mantle-derived helium and argon, suggests that these felsic plutonic rocks evolved from alkali basaltic magma that formed by partial melting of subcontinental lithospheric mantle beneath the back arc basin located along the active continental margin of the southeastern part of the Eurasian plate.

1. Introduction

The origin of felsic plutonic rocks and the possibility that felsic magmas are generated by fractional crystallization of mantle-derived alkali basaltic magma has been debated for many years. In recent times focus has been on the location and mechanism by which felsic plutonic rocks form and the insights which plutonic rocks may provide about subsurface magmatic processes (e.g., Dufek and Bergantz, 2005; Bonin and Bebien, 2005). Insights into the origin of felsic magmas have been made from the geochemical and isotopic characteristics of young (Neogene) felsic volcanic rocks from oceanic islands (e.g., Thirlwall et al., 1997; Bohrson and Reid, 1997; Kar et al., 1998; Kelemen et al., 2004). However, young felsic plutonic rocks are rarely found on the Earth's surface because it takes such a long time (≥0.8–1.9 Myr, (e.g., Harayama, 1992; Kar et al., 1998) for felsic magma to be emplaced, solidified and then exposed. Rare occurrences of felsic plutonic rocks are found in young volcanic, tectonic and geothermal areas such as in Eljurta, Caucasus Mountains (Lipman et al., 1993), the Crater Lake caldera, Oregon (Bacon et al., 2000; Bacon and Lowenstern, 2005), the Taupo, New Zealand (Charier et al., 2005), the Medicine lake volcano, California (Lowenstern et al., 2000), the

* Corresponding author.
E-mail address: kyuhan@ewha.ac.kr (K.H. Kim).

0009-2541/$ – see front matter © 2008 Elsevier B.V. All rights reserved.
doi:10.1016/j.chemgeo.2008.05.009

Ascension Island (Kar et al., 1998), the Japan Alps (Harayama, 1992), and The Geyser (Thompson, 1989; Dalrymple et al., 1999; Schmitt et al., 2003) and Larderello geothermal fields (Dini et al., 2005).

Recently, late Pleistocene (ca. 0.2 Ma, Rb–Sr and ^{40}Ar–^{39}Ar ages) felsic plutonic rocks (monzonites) have been found in tephra-dominated formations of the Ulleungdo volcanic island, South Korea. This unusual occurrence of felsic plutonic rocks in the tephra formation gives us important information about felsic (monzonitic) magmatism and the basement underlying the alkali volcanic province of a back arc basin.

Extensive noble gas studies on basaltic glasses and mineral separates from island arc settings have provided important insights into the formation mechanisms of arc and subduction-related volcanism, including the crustal contribution to magmatic systems, and the impact of recycling of subducted materials to the subduction zone mantle wedge (e.g., Hilton et al., 2002). In the case of back arc regions, noble gas analyses, especially on helium and argon, have been mostly conducted on submarine volcanic glasses of back arc basin basalts (e.g., Bach and Niedermann, 1993; Hilton et al., 1993; Macpherson et al., 1998; Sano et al., 1998; Marty et al., 2001) and ultramafic xenoliths from alkali basaltic rocks (e.g., Nagao and Takahashi, 1993; Sumino et al., 2000; Yamamoto et al., 2004; Kim et al., 2005). While the noble gas contents of volcanic-derived groundmasses are strongly depleted due to degassing and also are severely contaminated by atmosphere- and/or seawater-derived components, volatile-rich features such as vesicles within quenched pillow glass, and fluid inclusions within mantle xenoliths, do preserve noble gas compositions that formed at the time of eruption.

In contrast to comprehensive noble gas studies of back arc volcanic glasses and mantle xenoliths, silicate minerals from plutonic rocks have received only limited noble gas study. This is because there is a common view that radiogenic components such as ^{4}He and ^{40}Ar overwrite the primary magmatic signature that is inherited from the parental magma. The radiogenic compositions are produced from decay of U and Th-series and ^{40}K isotopes after cooling below the closure temperatures of these isotopes. In cases where a sample has been exposed to the Earth's surface for a geologically long time, noble gases isotopic ratios (especially helium and neon) are additionally disturbed by addition of a cosmic-ray produced component. Our extremely young age of the monzonites leads us to expect that post-solidification addition of a radiogenic component would be minimal; the original noble gas signature originated from their parental magma may well be preserved. Herein we document the occurrence of fragments of Ulleungdo monzonites, present their age and propose a petrogenetic model for the evolution of the extremely young plutonic rocks. As a new approach for understanding volcano-plutonic processes in back arc basins, we also discuss the origin and source characteristics of the felsic (monzonitic) magmas in terms of noble gas and Nd and Sr isotopes and whole rock geochemistry and the relationship between volcanic and plutonic rocks in a back arc basin located along the active continental margin of the southeastern corner of the Eurasian plate.

2. Geologic setting

The Ulleungdo is a submarine to subaerial dormant strato volcano (12 km × 10 km in size) with a small Nari caldera (2 km in diameter) at the summit. The Ulleungdo volcanic island is located in the central part of the back arc basin behind the Japanese island arc (Fig. 1). The volcanic history of this island is divided into five stages on the basis of lithology, occurrence and radiometric age. The stages are: Stage (1) 1.37–0.97 Ma, basaltic agglomerate; Stage (2) 0.83–0.77 Ma, trachyte; Stage (3) 0.73–0.24 Ma, trachyte; Stage (4) 9.8–6.3 ka, pumice and ash; and Stage (5)<6.3 ka, trachyandesite (Kim et al., 1999; Shiihara et al., 2004). Stage 3 can be subdivided into substages, 3U (0.24–0.47 Ma) and 3L (0.60–0.73 Ma). Most Ulleungdo volcanic rocks are characterized by extremely enriched alkali elements; i.e., K_2O+Na_2O range from 6.0 to 14.5 wt.% (av., 12.5 wt.%).

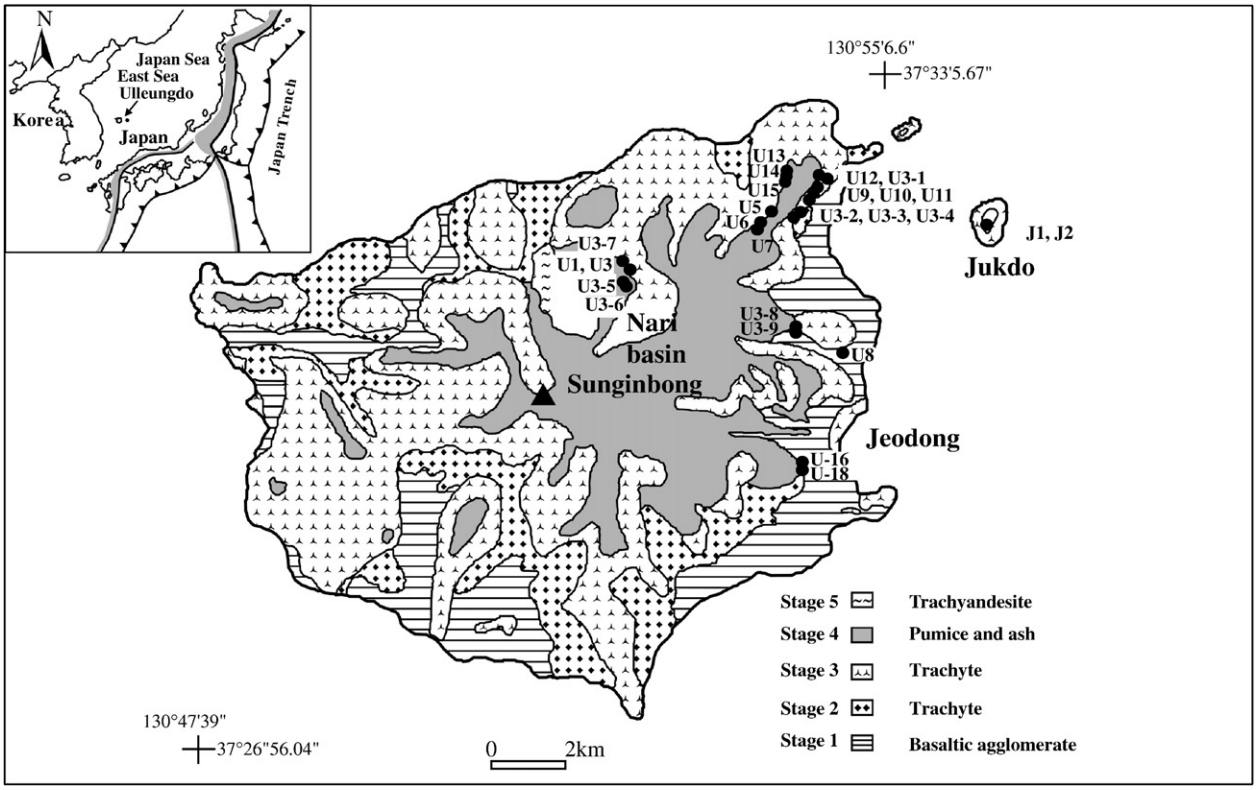

Fig. 1. Geologic map of the Ulleungdo volcanic island (Kim et al., 1999), showing the locations of sampling sites. Numerals indicate the sampling number (some samples were collected from the same site).

The Plinian style eruption of highly explosive high viscosity magma from the Ulleungdo occurred only during the Stage 4 eruptions, producing voluminous tephras that in detail included trachytic pumice, ash and small amounts of felsic (monzonitic) plutonic rock fragments and scoria. Near-vent tephra deposits around the Nari caldera (Nari basin) and the Suckpodong areas attain thickness of ca. 30–40 m and are generally homogeneous, and can be coarse containing large pumice fragments with 30 cm in diameter. Small sized-andesite and basaltic rock fragments were found rarely in tephras. The tephras are characterized by the trachytic composition. The Ulleungdo trachytes contain considerable amounts of alkali feldspar, kaersutite, biotite and clinopyroxene as phenocrysts, and the alkalic composition of volcanic glasses ranging from 13 to 14 wt.% in K_2O+Na_2O (Shiihara et al., 2004).

Felsic plutonic blocks are included only in the U-4 subunit of the tephra sequence of Stage 4. Large subround to angular plutonic blocks, varying in size from a few centimeters to 35 cm in length, consist mainly of coarse-grained hornblende biotite monzonite and syenite, and medium to fine-grained hornblende monzonite. The plutonic rocks are equigranular and are composed mainly of alkali feldspar, plagioclase, hornblende, and biotite with minor amounts of quartz and opaque minerals. Under the polarizing microscope, some alkali feldspars show perthitic texture. The simple twining, the Carlsbad twin, is very common in monoclinic alkali feldspar and plagioclase.

3. Analytical procedures

Major and minor elements in powdered fresh bulk rocks were analyzed by X-ray fluorescence spectrometry (Shimazu XRF-17000) at Bukyong University, Korea. Trace element concentrations were determined by ICP-mass spectrometer (Perkin Elmer, Elan 6100) at the Korea Ocean Research and Development Institute, Korea. The precisions for major element results are better than 5% and 10% for trace elements. Standard reference materials for major elements were BIR-1 (basalt), RGM-1 (rhyolite), STM-1 (syenite), and SARM 1 (granite). For the trace element analysis, the standard reference materials BHVO-2 (basalt), JG-2 (granite), AGV-1 (andesite) and JG-3 (granodiorite) were used.

For the purpose of Nd and Sr isotopic measurement, ca. 0.1 g of powder sample was digested by the standard acid mixture. The sample solution was split into two portions: one for natural isotopic ratio measurement and another for determining the abundance of Rb, Sr, Sm, and Nd. These isotopic ratios were measured on a VG sector thermal ionization mass spectrometer at Nagoya University, Japan. The obtained $^{87}Sr/^{86}Sr$ and $^{143}Nd/^{144}Nd$ were normalized to $^{86}Sr/^{88}Sr=0.1194$ and to $^{146}Nd/^{144}Nd=0.7219$, respectively. Reported uncertainties on the current results are 2SE of the mean of 200 ratios. Reference materials were measured with unknown samples. Replicate analyses of NBS-987 and JNdi-1 standards gave $^{87}Sr/^{86}Sr=0.710244\pm19$ ($N=28$, 2σ) and $^{143}Nd/^{144}Nd=0.512105\pm14$ ($N=18$, 2σ). The Rb, Sr, Sm and Nd concentrations were determined by an isotopic dilution method with a Finigan MAT thermoionic quadrupole mass spectrometer (THQ) at the same university. Uncertainties for abundance of above elements are less than 1% on repeated analyses of the rock reference samples.

For the K–Ar and Ar–Ar dating of the monzonites, hornblende and biotite were separated from monzonites by hand picking under binocular microscope. Separated mineral samples for Ar–Ar were wrapped in aluminum foil with flux monitors biotite (EB-1), K_2SO_4 and CaF_2. Samples' irradiation was done at the JMTR reactor. During the irradiation, samples were shielded by Cd foil in order to reduce thermal neutron-induced ^{40}Ar from ^{40}K. The Ar extraction and Ar isotopic analyses were carried out at Radioisotope Center, University of Tokyo. During incremental heating, gases were extracted in 12 steps between 400 and 1500 °C using the analytical method by Ebisawa et al. (2004). Ar isotope analysis for K–Ar dating was done by a sensitivity method without ^{38}Ar-spike using a modified VG5400 mass spectrometer (MS-III) at the Laboratory for Earthquake Chemistry (LEC), University of

Table 1
K–Ar ages of Ulleungdo monzonite clasts

Sample no.	K (wt.%)	wt (g)	^{40}Ar radiogenic 10^{-8}ccSTP/g	^{36}Ar 10^{10}ccSTP/g	Age (Ma)	Air (%)
U1 (Hb)	1.16	0.024	2.66±0.64	5.35±0.20	0.59±0.14	85.6
U10 (Hb)	0.09	0.016	10.28±1.59	15.02±0.58	28.25±4.41	81.2
U12 (Hb)	1.39	0.232	1.96±0.10	3.82±0.19	0.363±0.022	85.2
U6 (Hb)	2.67	0.207	16.62±0.84	18.03±0.90	1.602±0.094	76.3
U6 (Bi)	6.71	0.088	5.60±0.32	37.07±1.86	0.215±0.014	95.2
U6B (Bi)	6.99	0.120	5.04±0.27	35.20±1.76	0.186±0.012	95.4

Hb: hornblende, Bi: biotite. Samples were analyzed at the Laboratory for Earthquake Chemistry, University of Tokyo, Japan (U6A, U6B, U12) and the Korea Basic Science Institute, Korea (U1, U10). U6B is collected from the same site of U6.

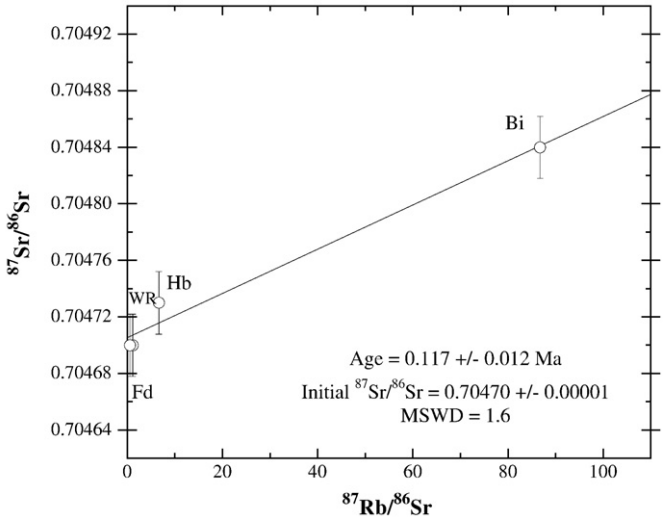

Fig. 2. Rb–Sr mineral isochron for Ulleungdo hornblende–biotite monzonite (U6). All error bars are 2σ uncertainties, and are given only where they exceed the size of the symbol in the plot. Bi: biotite, Hb: hornblende, Fd: feldspar, WR: whole rock. (Isotopic data are listed in Table 5).

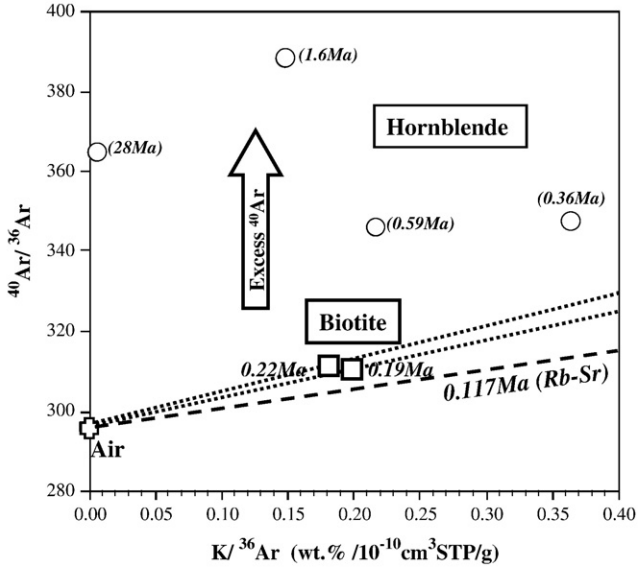

Fig. 3. Plot for $^{40}Ar/^{36}Ar$ versus $K/^{36}Ar$ in biotite and hornblende minerals from the monzonites. Hornblende minerals clearly show ^{40}Ar excess.

Tokyo, Japan. K-concentration was determined by an atomic absorption spectrophotometer with 5% analytical precision at the LEC.

Noble gases were extracted from mineral grains in the monzonites using the *in vacuo* crushing and heating method. The crushing method is able to distinguish the trapped magmatic noble gas component, as radiogenic and cosmogenic isotopes remain close to their production sites within the mineral's crystal lattice (e.g., Kurz, 1986). However, intense crushing would release the radiogenic/cosmogenic component (Hilton et al., 1993; Scarsi, 2000; Yokochi et al., 2005). Consecutive melting of crushed and powdered samples ('powder melting') enabled us to evaluate the amount of post-eruptive secondary components in the mineral lattice. Additionally, we applied a two-step sequential crushing to one sample to verify possible release of the secondary components by our crushing method. In the crushing experiments, ca. 30–70 mg of mineral separates (hornblende, biotite and feldspar) were crushed in a stainless steel tube by 2000 strokes of a nickel rod driven from outside the vacuum by a solenoid magnet. The crushed samples were recovered from the crusher and completely melted at 1800 °C to extract all noble gases present in the mineral lattices and possibly in remaining fluid inclusions. The isotopic compositions of the released noble gases were measured using a sector-type mass spectrometer, a modified VG5400 in the LEC at the University of Tokyo. The discrimination factor for $^{3}He/^{4}He$ was determined using HESJ (the He Standard of Japan), with $^{3}He/^{4}He = (28.88 \pm 0.14) \times 10^{-6}$ (Matsuda et al., 2002). Full details of the gas extraction and basic analytical procedure are described in Sumino et al. (2001). Experimental uncertainties in the noble gas concentrations were estimated to be about 10% based on the reproducibility of the measurements of gas from each sample. Errors on isotopic ratios incorporate errors in blank correction and mass discrimination and are quoted at one standard deviation.

4. Results

4.1. Radiometric ages

Radiometric age determinations were made on biotite and hornblende, separated from representative monzonites, using the Rb–Sr mineral isochron, and the K–Ar and Ar–Ar method.

4.1.1. Rb–Sr isochron ages

The isochron was calculated by ISOPLOT program (Ludwig, 1991). Mineral isochron for hornblende, biotite, feldspar and whole rock (U6) gives an age of 0.117±0.012 Ma with an initial $^{87}Sr/^{86}Sr$ ratio of

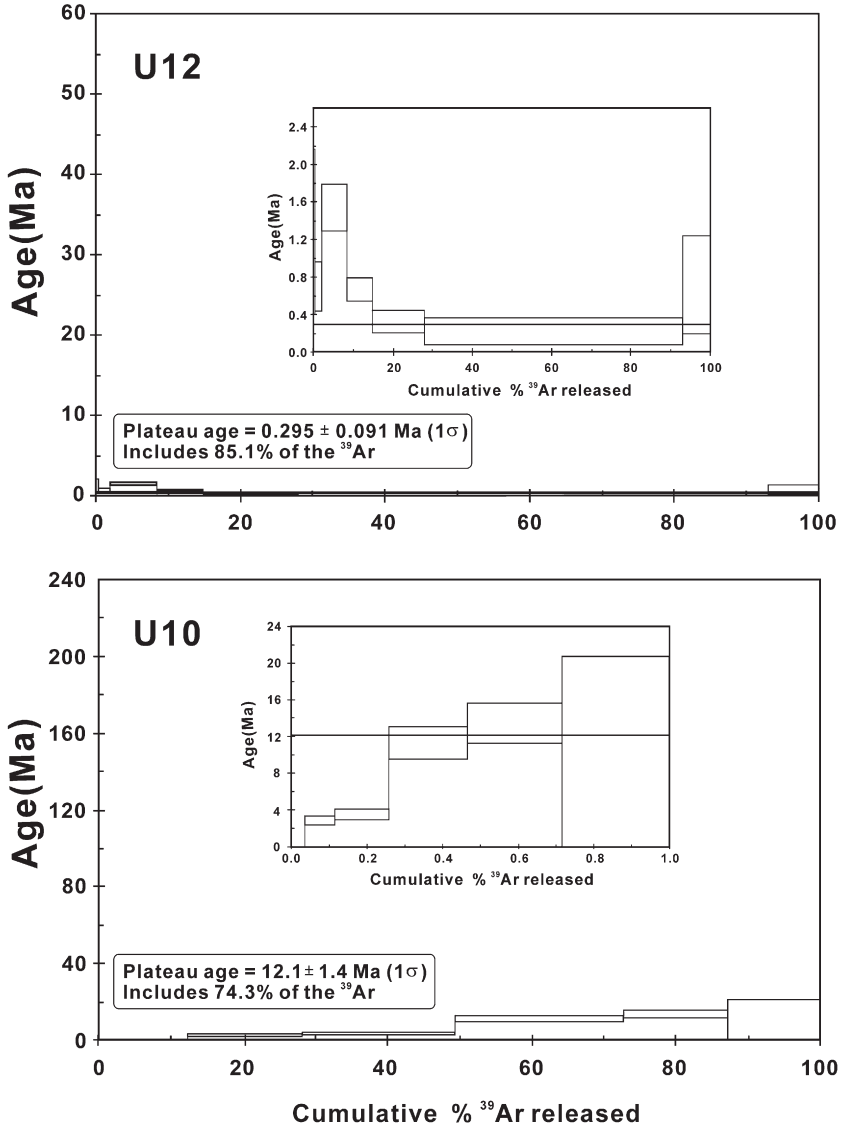

Fig. 4. $^{40}Ar/^{39}Ar$ age spectra for hornblendes from the Ulleungdo monzonites. Error for each step is given in 2σ level, whereas plateau ages are given at the 1σ level. Inside box indicates enlarged diagram.

Table 2
Radiometric age data for post-Pleistocene plutonic rocks on Earth

Unit name	Rock type	K–Ar age (Ma)	Rb–Sr age (Ma) (mineral isochron)	U–Pb age (Ma)	Reference
<Unexposed plutonic rock>					
Ulleungdo (South Korea)	Monzonites	0.19–0.22 (0.29)	0.12		Present study
Crater Lake Caldera, Oregon	Granodiorite			0.10–0.17	Bacon et al. (2000)
Crater Lake Caldera, Oregon	Granodiorite			0.02–0.30	Bacon and Lowenstern (2005)
Taupo, New Zealand	Crystallised Crystallized body (zircon)			0.51	Charier et al. (2005)
Medicine Lake volcano, California	Granitoid xenolith			0.025–0.09	Lowenstern et al. (2000)
The Geysers, California	Granite			1.27	Schmitt et al. (2003)
The Geysers, California	OPX–bi granite			0.67–1.22	Dalrymple et al. (1999)
Ascension Island (South Atlantic ocean)	Granite zenoliths		0.9–1.2		Kar et al. (1998)
The Geysers field (USA)	Felsite (granite)	0.9–2.4			Thompson (1989)
Larderello (Italy)		(1.0–3.8)			Dini et al. (2005)
<Exposed plutonic rock>					
Takidani (Central Japan)	Granodiorite	0.8–1.9			Harayama (1992)
Aboyama (Central Japan)	Quartz diorite	0.9			Harayama (1990)
Yakuradake (Central Japan)	Quartz diorite	1.1–1.2			Kurasawa et al. (1989)
Eldjurta Caucasus Mt. (Russia)	Granite	1.0–2.8			Lipman et al. (1993)

Numerals in parenthesis indicate $^{40}Ar/^{39}Ar$ data.

0.704706±0.000009 (2σ) (Fig. 2). The small uncertainty is resulted from fortuitous that the data points are on a correlation line. Hornblende granite sample (U9) yields the mineral isochron age of 0.27±0.23 Ma with an initial $^{87}Sr/^{86}Sr$ ratio of 0.704700±0.00001 (2σ). The two isochrons show relatively concordant ages and provide unusually young ages for plutonic rocks.

4.1.2. K–Ar ages

Two biotites from the monzonite samples U6 and U6B also yield very young K–Ar cooling ages of 0.19 and 0.22 Ma (Table 1), reflecting their respective closure temperatures (370–400 °C). However, K–Ar ages for four hornblende samples from the monzonites clearly show the effects of ^{40}Ar excess (Fig. 3) and give rise to older ages ranging from 0.36 to 28.3 Ma (Table 1). The presence of magmatic helium ($^{3}He/^{4}He = 6.0\ R_A$) in the hornblende sample (U12), which is obtained by *in vacuo* crushing experiment, indicates that the above older hornblende ages are due to excess Ar (see Table 6). Excess Ar corrected age of 0.20 Ma for the hornblende sample (U12) with an assumption of initial $^{40}Ar/^{36}Ar$ of 320, which is estimated value from the crushing experiment, is close to the Rb–Sr isochron and K–Ar biotite ages. Considering the possible effect of excess ^{40}Ar on the biotite ages, real K–Ar ages for the monzonites must be less than the apparent ages of 0.2 Ma.

Table 3
Sampling location, and major element and normative mineral compositions for representative Ulleungdo monzonites

Sample no.	U1	U3	U5	U6	U7	U8	U9	U10	U11	U12	U13	U14
Latitude (N)	37°31′18″	37°31′18″	37°31′50″	37°31′45″	37°31′40″	37°30′33″	37°32′4″	37°32′1″	37°31′56″	37°32′10″	37°32′13″	37°32′10″
Longitude (E)	130°52′15″	130°52′15″	130°53′53″	130°53′46″	130°53′44″	130°54′39″	130°54′22″	130°54′20″	130°54′18″	130°54′24″	130°54′3″	130°54′3″
Major elements (wt.%)												
SiO_2	60.96	63.18	57.10	59.85	60.01	61.83	62.22	60.87	61.74	59.18	61.16	61.03
Al_2O_3	18.74	19.59	18.65	18.34	18.99	19.19	19.73	19.52	18.36	18.93	18.85	18.73
TiO_2	0.28	0.18	0.92	0.81	0.49	0.29	0.24	0.29	0.29	0.65	0.29	0.39
Fe_2O_3	4.05	2.35	5.17	4.18	3.91	4.10	2.26	3.52	4.83	3.76	3.18	4.39
MnO	0.19	0.10	0.14	0.13	0.16	0.17	0.13	0.18	0.19	0.11	0.15	0.13
MgO	0.22	0.09	1.37	0.79	0.38	0.13	0.15	0.19	0.31	0.61	0.16	0.46
CaO	1.48	1.18	3.08	1.70	1.48	1.10	0.83	1.19	1.35	1.99	1.15	1.59
Na_2O	6.94	6.99	6.26	5.73	6.73	6.83	7.53	7.87	6.73	6.18	7.15	5.48
K_2O	6.15	6.53	5.71	6.44	6.57	5.90	6.72	6.32	5.96	6.65	6.33	6.70
P_2O_5	0.05	0.02	0.27	0.19	0.08	0.01	0.03	0.02	0.06	0.17	0.02	0.08
Total	99.06	100.21	98.67	98.16	98.81	99.55	99.84	99.97	99.82	98.23	98.44	98.98
CIPW norm												
q	–	–	–	–	–	–	–	–	–	–	–	–
or	36.34	38.59	33.74	38.06	38.83	34.87	39.71	37.35	35.22	39.30	37.41	35.59
ab	47.53	49.57	39.13	46.29	42.63	51.96	45.52	42.87	51.55	40.56	47.09	46.37
an	1.82	2.79	5.92	5.30	2.20	4.28	0.19	–	2.29	4.27	0.64	6.72
ne	6.06	5.19	7.50	1.19	7.76	3.16	9.86	12.11	2.93	6.36	7.26	–
di	1.18	0.48	3.84	–	2.04	0.60	0.81	1.02	1.67	2.07	0.86	–
hy	–	–	–	–	–	–	–	–	–	–	–	0.43
wo	1.44	0.87	–	–	0.38	–	0.99	1.74	0.67	–	1.42	–
ol	–	–	1.14	1.38	–	0.03	–	–	–	0.39	–	0.50
ac	–	–	–	–	–	–	–	1.21	–	–	–	–
mt	–	–	–	–	–	–	–	–	–	–	–	–
il	0.41	0.21	0.30	0.28	0.34	0.36	0.28	0.39	0.41	0.24	0.32	0.28
hem	4.05	2.35	5.17	4.18	3.91	4.10	2.26	3.10	4.83	3.76	3.18	4.39
ap	0.12	0.05	0.63	0.44	0.19	0.02	0.07	0.05	0.14	0.39	0.05	0.19
tn	–	–		–	–	–	–	–	–	–	–	0.45
pf	0.11	0.11	1.30	0.92	0.53	0.17	0.16	0.15	0.13	0.90	0.21	–
ru	–	–	–	0.15	–	–	–	–	–	–	–	0.07
Total	99.06	100.21	98.67	98.19	98.81	99.55	99.85	99.99	99.84	98.24	98.44	94.99

4.1.3. Ar–Ar ages

The $^{40}Ar/^{39}Ar$ technique has been used here to detect any perturbation since solidification and thereby to check the validity of the K–Ar ages for these samples. For comparison, three same samples (U1, U10, U12) were used in K–Ar and Ar–Ar dating. $^{40}Ar/^{39}Ar$ apparent ages were plotted against cumulative percentage ^{39}Ar released (Fig. 4). $^{40}Ar/^{39}Ar$ plateau ages were obtained to be 0.03±0.08 Ma (U1), 0.29±0.09 Ma (U12) and 12.1±1.4 Ma (U10), in good agreement with determinations by excess argon corrected ages of 0.24 Ma (U1), 0.20 Ma (U12) and 10.6 Ma (U10). However, sample U1 failed to yield a reliable age spectrum due large errors. Hornblende sample U12 yields an age spectrum that is characterized by disturbed release spectrum at low temperature, suggesting the presence of excess argon (Fig. 4). On the other hand, age spectrum of sample U10 shows a diffusion loss profile. Our radiometric dating results indicate that the onset of Ulleungdo felsic plutonism is coeval with extremely young volcanism in this island except one sample U10 (28.2 Ma) (Table 1).

The relatively concordant ages described above are the plausible solidifying age of the Ulleungdo felsic (monzonitic) magma. It is interesting to note that these ages overlap with the timing of the Ulleungdo substage 3U eruption involving alkali volcanic magmatism (0.24–0.47 Ma, Kim et al., 1999).

The radiometric ages (0.12–0.29 Ma) determined by the Rb–Sr mineral isochron, the Ar–Ar and K–Ar dating indicate that we have found monzonites with one of the extremely young age of plutonic rocks on Earth (Table 2). The new exceptionally young radiometric ages of Ulleungdo monzonites provide us with important new insights on the generation of felsic magma, the relationship between volcanic and plutonic rocks, the evolution of alkali basaltic magma and the tectonic and crustal evolution of a back arc basin.

4.2. Geochemistry of the Ulleungdo felsic plutonic rocks

Major elements with their normative values for twenty six felsic plutonic rock samples are presented in Table 3. The CIPW norm for the plutonic rocks approaching to zero in quartz and to equal amounts of alkali feldspar (31.38–42.56%) and plagioclase (35.92–59.89%) can be classified as monzonites on IUGS classification of plutonic rocks (Le Maitre et al., 1989). A general view of the variation of oxide concentrations with silica is shown in Fig. 5. The Ulleungdo felsic plutonic rocks have a silica oversaturated alkali compositions (57–63 wt.%). Total alkali contents (K_2O+Na_2O) range from 10.74 to 14.65 wt.% (av., 12.5 wt.%), similar to the alkali contents of so-called A-type granites (Eby, 1990) and of Ulleungdo alkali volcanic rocks (K_2O+Na_2O= 5.95–14.15, av., 12.6 wt.%, Kim et al., 1999). Meanwhile, CaO and MgO contents are lower than those of Mesozoic and Cenozoic granites from the inland of the Korean peninsula. The Ulleungdo felsic rocks show the peraluminous character with Al_2O_3 of 17.21 to 20.93 wt.% and a wide compositional variation with the TiO_2 (0.08–1.24 wt.%) and P_2O_5 (0.01–0.36 wt.%) contents as shown in Table 3 and Fig. 5. The MgO, Fe_2O_3, TiO_2 and CaO contents decrease with increasing of the silica content, whereas the K_2O and Na_2O contents show a positive trend. The felsic plutonic rocks generally plot on the most evolved end major element fractionation trends defined by the volcanic rocks.

Ulleungdo monzonites have extremely wide variation in trace element abundance as shown in Table 4 and Fig. 6. For example Zr/Nb in monzonites as compared with the trachytic rocks (Zr/Nb=3.8–5.0, av., 4.2) ranges from 2.1 to 10 (av., 4.2), which are probably due to zircon fractional crystallization. The most significant features of the Ulleungdo monzonites are the similar geochemical characteristics to the alkali volcanic rocks in the Ulleungdo, which show almost the same concentrations of major, trace and rare earth elements. As shown in Table 4, the monzonites with low Y/Nb ratios (0.03–0.32)

U15	U16	U18	U3-1	U3-2	U3-3	U3-4	U3-5	U3-6	U3-7	U3-8	U3-9	J1	J2
37°32′6″	37°29′33″	37°29′29″	37°32′9″	37°31′51″	37°31′48″	37°31′48″	37°31′12″	37°31′9″	37°31′23″	37°30′48″	37°30′44″	37°31′43″	37°31′43″
130°54′2″	130°54′13″	130°54′13″	130°54′29″	130°54′13″	130°54′′9″	130°54′9″	130°52′10″	130°52′12″	130°52′10″	130°54′7″	130°54′6″	130°56′14″	130°56′14″
56.66	60.29	58.42	60.14	59.05	58.56	62.56	60.68	60.27	58.22	60.76	62.78	59.92	57.83
18.57	18.58	19.21	18.44	17.47	18.46	19.46	17.99	18.79	17.21	19.38	19.00	17.44	20.93
1.24	0.35	0.08	0.45	1.03	0.78	0.10	0.83	0.74	0.93	0.42	0.51	0.86	0.24
6.49	3.06	4.71	3.81	5.64	4.62	3.59	4.66	3.98	6.86	3.02	2.14	5.20	2.34
0.20	0.12	0.25	0.14	0.16	0.13	0.11	0.15	0.12	0.21	0.08	0.08	0.17	0.15
1.59	0.04	0.07	0.47	1.22	0.90	0.04	0.53	0.83	1.38	0.47	0.24	0.85	0.22
3.15	0.69	0.85	1.45	2.20	2.43	0.97	1.34	2.06	2.39	2.15	1.38	2.01	0.98
5.43	7.63	9.16	6.08	5.22	5.78	7.63	5.67	5.75	4.91	5.31	5.47	5.19	8.82
5.31	6.39	5.48	6.53	6.36	6.47	5.24	6.79	6.59	6.81	6.75	7.20	6.96	5.99
0.44	0.04	0.02	0.13	0.26	0.21	0.01	0.10	0.21	0.36	0.11	0.10	0.27	0.04
99.08	97.20	98.87	97.62	98.61	98.34	99.72	98.74	99.35	99.28	98.45	98.91	98.87	97.56
–	–	–	–	–	–	–	–	–	–	–	0.41	–	–
31.38	37.76	32.38	38.59	37.58	38.23	30.97	40.13	38.94	40.24	39.89	42.55	41.13	35.40
43.73	42.36	36.20	45.57	44.17	40.59	56.52	47.40	44.63	41.01	44.40	46.29	43.92	35.92
10.61	–	–	3.74	5.45	5.32	3.37	3.58	6.00	4.81	9.11	6.03	3.73	–
1.20	9.55	17.39	3.19	–	4.51	4.36	0.31	2.18	0.29	0.29	–	–	20.79
–	0.21	0.38	1.24	0.63	2.46	0.21	0.09	0.58	1.78	–	–	1.67	1.18
–	–	–	–	0.61	–	–	–	–	–	–	0.60	–	–
–	0.89	1.50	–	–	–	0.46	–	–	–	–	–	–	1.18
2.77	–	–	0.42	1.50	0.77	–	0.90	1.26	1.83	0.82	–	0.94	–
–	4.03	8.11	–	–	–	–	–	–	–	–	–	–	0.29
–	–	0.58	–	–	–	0.07	–	–	–	–	–	–	–
0.43	0.26	0.15	0.30	0.34	0.28	0.19	0.32	0.26	0.45	0.17	0.17	0.36	0.32
6.49	1.67	1.50	3.81	5.64	4.62	3.54	4.66	3.98	6.86	3.02	2.14	5.20	2.24
1.02	0.09	0.05	0.30	0.60	0.49	0.02	0.23	0.49	0.83	0.25	0.23	0.63	0.09
–	–	–	–	2.09	–	–	–	–	–	–	0.12	0.50	–
1.05	0.37	–	0.50	–	1.08	–	1.13	1.03	1.18	0.41	–	0.79	0.12
0.51	–	–	–	–	–	–	–	–	–	0.11	0.47	–	–
99.19	97.19	98.24	97.66	98.61	98.35	99.71	98.75	99.35	99.28	98.47	99.01	98.87	97.53

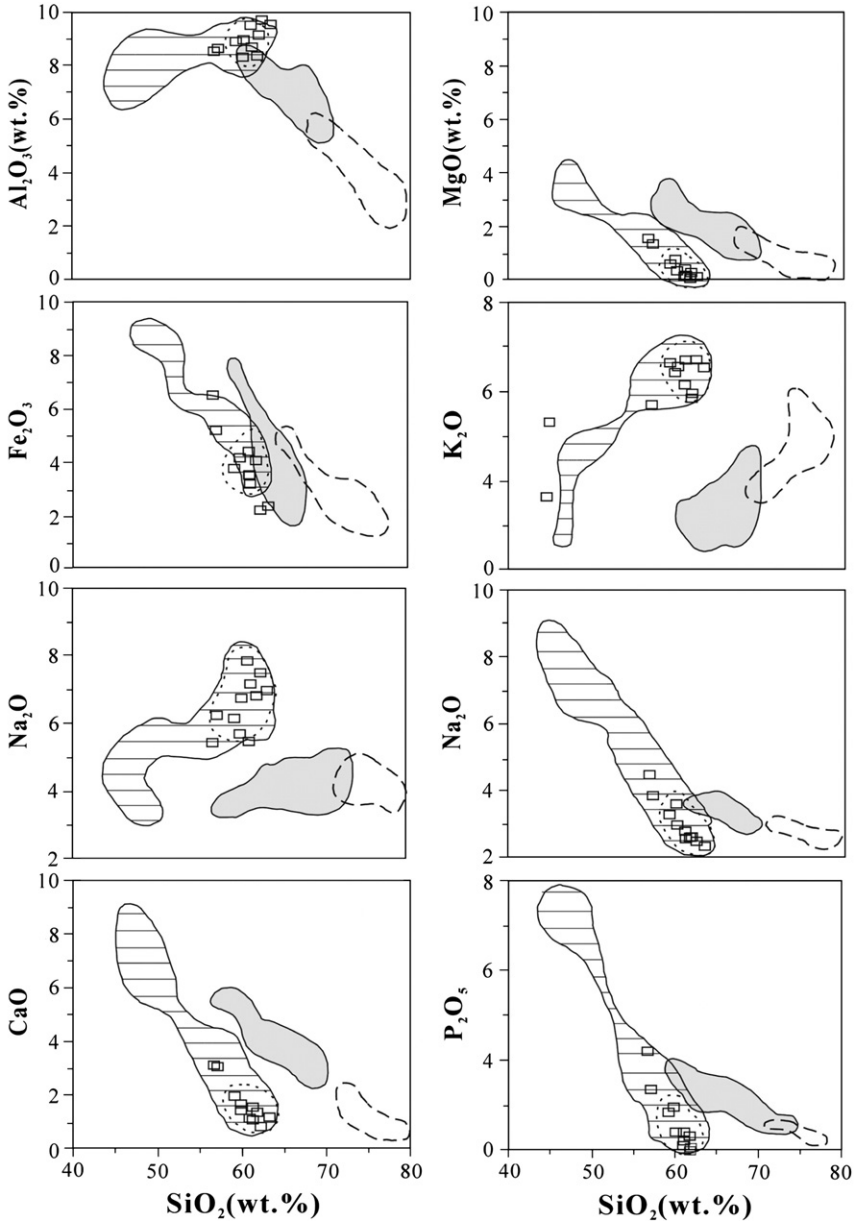

Fig. 5. Plots of major oxides versus SiO_2 for Ulleungdo monzonites. The shaded and dashed fields indicate Daebo and Bulguksa granites, respectively (Kim, 1992). The slashed area is alkali volcanic rocks from the Ulleungdo (Kim et al., 1999). Dotted line in slashed area shows Stage 3 of the Ulleungdo volcanics.

could be derived from sources chemically similar to those of oceanic island basalts (Y/Nb<1.2) (Eby, 1990), like the Ulleungdo alkali volcanic rocks (Y/Nb=0.14–0.32) (Kim et al., 1999). REE concentrations (∑REE) vary widely from 69 to 336 ppm (Table 4). LREE in the monzonites are more enriched than HREE (LREE/HREE=14–23), reflecting the incorporation of alkali (OIB type) magma. In addition to trace elements, REE abundance of the monzonites is also similar to those of the alkali volcanics in the Ulleungdo but a little lower REE abundances. The REE abundance pattern of the Ulleungdo volcanic rocks suggests that volcanic rocks of the Stage 3 originated from identical parent alkali basaltic magma (Kim et al., 1999).

4.3. Nd and Sr isotopes

Analytical results of Nd and Sr isotopes with Rb, Sr, Sm and Nd concentrations for Ulleungdo monzonites are listed in Table 5. Strontium isotopes for the monzonites show a wide variation ranging from 0.70454 to 0.71264 ($\varepsilon Sr(t)$=0.1~ −101). In contrast to the Sr isotopes, the monzonites have nearly constant $^{143}Nd/^{144}Nd$ ratios ranging from 0.512527 to 0.512577 with $\varepsilon Nd(t)$ values ranging from −1.2 to −2.2 (Table 5). The isotopic data require a sea water component, in addition to probable continental crustal contribution to produce the Ulleungdo felsic (monzonitic) magma.

In addition to isotopic ratios, it is noteworthy that the Ulleungdo monzonites contain a significantly variable and low concentration of strontium (1.8–331.8 ppm av., 128.6 ppm) (Table 5). The Rb concentrations of the monzonites also vary from 108.1 to 251.3 ppm with the wide Rb/Sr ratios ranging from 0.4 to 95.1 as shown in Table 5. The Sr concentrations combined with Sr isotopic ratios of whole rock monzonite samples from the Ulleungdo allow us to group the samples into two types (Table 5 and Fig. 7). Type 1: low initial $^{87}Sr/^{86}Sr$ ratios (0.70454–0.70593) with relatively high Sr and low Rb concentrations (Rb/Sr=0.4–8.8). Type 2: high initial $^{87}Sr/^{86}Sr$ ratios (0.70729–0.71264) with extremely low concentrations of Sr and high concentrations of Rb (Rb/Sr=67.4–95.1). Type 1 monzonites characterized by comparatively low $^{87}Sr/^{86}Sr$ ratios may reflect dominant mantle mantle-

Table 4
Trace and rare earth element concentrations for representative Ulleungdo monzonites

Sample no.	U1	U6	U7	U8	U9	U10	U12	U14	U15	U16	J1
Trace elements (ppm)											
Ba	648	997	322	97.7	410	318	585	350	287	291	133
Ce	53.7	133	158	37.0	72.7	109	64.4	82.0	39.6	76.8	67.2
Co	0.6	3.1	2.0	0.6	0.9	0.4	3.3	2.3	1.4	0.4	1.2
Cr	4.2	39.4	5.3	1.6	3.1	5.6	8.6	15.7	4.8	6.9	4.5
Nb	88.0	102	133	41.2	98.6	123	94.7	123	25.3	93.9	35.2
Ni	2.8	18.9	2.3	0.7	1.1	1.3	3.9	89.5	2.3	2.8	1.2
Rb	174	128	108	150	226	183	109	133	35.1	196	75.1
Sr	1.8	308	247	71.2	25.7	2.01	219	85.7	110	2.8	40.7
V	1.8	14.8	7.3	2.4	5.9	0.6	16.0	4.9	9.3	1.0	1.9
Y	2.7	25.3	24.1	5.6	18.4	12.8	8.9	11.1	7.0	9.1	11.3
Zn	25.9	77.5	76.6	25.9	65.7	96.4	91.7	54.1	43.8	67.5	43.8
Zr	278	378	679	279	990	367	236	270	107	259	114
REE (ppm)											
La	6.4	72.3	93.5	21.2	48.7	58.8	32.6	35.6	18.2	49.4	39.6
Ce	53.7	132.6	158.2	37.0	72.7	108.7	64.4	82.0	39.6	76.8	67.2
Pr	1.5	12.8	14.4	2.8	6.3	8.9	4.7	6.4	3.3	6.4	6.8
Nd	20.7	33.01	68.11	3.30	20.73	10.63	12.89	22.0	11.6	50.33	25.4
Sm	3.09	4.77	10.33	1.98	3.08	1.78	2.11	3.4	1.9	6.62	4.1
Eu	0.2	2.4	0.9	0.3	0.5	0.3	1.1	0.8	0.6	0.3	1.5
Gd	0.7	7.0	7.1	1.4	3.3	4.1	2.7	3.6	1.9	3.0	4.0
Dy	0.8	4.7	4.4	1.1	2.7	2.5	1.8	2.4	1.4	1.8	2.4
Ho	0.2	0.8	0.8	0.2	0.5	0.4	0.3	0.4	0.2	0.3	0.4
Er	0.4	2.4	2.4	0.6	1.9	1.4	1.0	1.3	0.7	1.0	1.1
Tm	0.0	0.3	0.3	0.1	0.3	0.2	0.1	0.1	0.1	0.1	0.1
Yb	0.5	1.8	2.2	0.6	2.1	1.3	0.9	1.1	0.6	0.9	0.8
Lu	0.2	0.2	0.3	0.1	0.3	0.2	0.1	0.2	0.1	0.1	0.1
LREE/HREE	22.9	15.6	18.2	17.6	13.6	20.6	17.7	16.5	14.9	21.4	16.3
Y/Nb	0.03	0.25	0.18	0.14	0.19	0.10	0.09	0.09	0.28	0.10	0.32
Zr/Nb	3.1	3.7	5.1	6.8	10.0	2.9	2.5	2.1	4.3	3.2	2.8

Rb, Sr, Sm, and Nd concentrations for sample nos. U1, U6, U7, U8, U9, U10, U12, and U18 were determined isotopic dilution methods.

derived source materials. On the other hand, monzonites of Type 2 having relatively high initial $^{87}Sr/^{86}Sr$ ratios may indicate a significant contribution of crustal materials and/or sea water to the monzonitic magma. Interestingly, Kim et al. (1999) proposed that Stage 3 Ulleungdo volcanics underwent seawater alteration and crustal contamination based on the wide initial $^{87}Sr/^{86}Sr$ isotopic variation of the alkali volcanic rocks which range from 0.7038 to 0.7092. The present isotopic data as well as Sr concentrations of the monzonites fall within the same ranges of Ulleungdo Stage 3 alkali volcanic rocks (Fig. 8). The Rb concentrations of the Stage 3U and 3L alkali volcanic rocks range from 97 to 165 ppm and 135 to 228 ppm, respectively (Kim et al., 1999). Their Sr abundances range from 244 to 1211 ppm and 10 to 319 ppm, respectively. The isotopic composition and Rb and Sr concentrations of Type 1 Ulleungdo monzonites resemble those of the alkali volcanic rocks of substages 3U (0.24–0.49 Ma). Meanwhile, the isotopic composition and Rb and Sr concentrations of Type 2 monzonites are closely correlated with those of substage 3L (0.60–0.73 Ma) volcanic rocks. These isotopic signatures can best be explained if the source of the monzonitic magma is identical to the source of trachytic magma formed during substage 3U and 3L.

4.4. Noble gas isotopes

Helium and argon isotope results from sixteen silicate mineral separates (hornblende, biotite, and feldspar) from seven Ulleungdo monzonite clasts are summarized in Table 6. Neon isotopes, and the abundances of neon, krypton and xenon, are presented in Table 7. Total ^4He concentrations in hornblende show a widely variable range from 6 to 99×10^{-8} cm^3STP/g. Biotite samples contain less ^4He ($3–7\times10^{-8}$ cm^3STP/g). Significantly low ^4He concentrations were observed in feldspar, with a range of $0.3–0.7\times10^{-8}$ cm^3STP/g. Approximately 30–80% of total helium was extracted by the crushing stage. $^3He/^4He$ ratios range from 0.5 to 6.5 R_A ($R_A = 1.40\times10^{-6}$, Mamyrin et al., 1970) in the crushing experiment, whereas those in the powder melting experiment show a wider range from 2 to 30 R_A (Fig. 9).

Total ^{36}Ar concentrations of the three kinds of silicate minerals vary widely from 6 to 61×10^{-10} cm^3STP/g. $^{40}Ar/^{36}Ar$ ratios obtained with the crushing extraction range from 307 to 1243, while those produced by powder melting range from 298, close to the atmospheric ratio (296.0, Nier, 1950), to 453. Systematically low $^{40}Ar/^{36}Ar$ ratios in each sample that was processed via the powder melting stage are due to contamination by atmospheric heavy noble gases adsorbed on fresh grain surfaces, as can be seen in the enrichment of ^{36}Ar, ^{84}Kr, and ^{132}Xe (Tables 6 and 7) (e.g., Niedermann and Eugster, 1992). Most $^{38}Ar/^{36}Ar$ ratios are identical within 2σ error, to the atmospheric ratio (0.1880) with the exception of some data obtained using crushing and powder melting. These exceptions are associated with fractionation of neon that has resulted in an enrichment of lighter isotopes (data shown in Table 7), suggesting that both isotope anomalies can be explained by mass fractionation of diffusive gas (Kaneoka, 1980).

5. Discussion

5.1. Helium components in the samples

Relatively uniform $^3He/^4He$ ratios around 6 R_A were obtained by the crushing of hornblende and biotite minerals (Fig. 9). The $^3He/^4He$ ratios of these samples clearly indicate a presence of mantle-derived helium enriched in ^3He, which is trapped in fluid inclusions. Hornblende and biotite samples concentrate on the 1:1 correlation line of Fig. 9, indicating either that helium extracted by the powder melting must be dominated by the trapped component in those fluid inclusions that survived the crushing stage, and/or that helium dissolved in the crystal matrix has similar $^3He/^4He$ ratios to that in the fluid inclusions, with a minor contribution of cosmogenic/radiogenic components (Hilton et al., 1993).

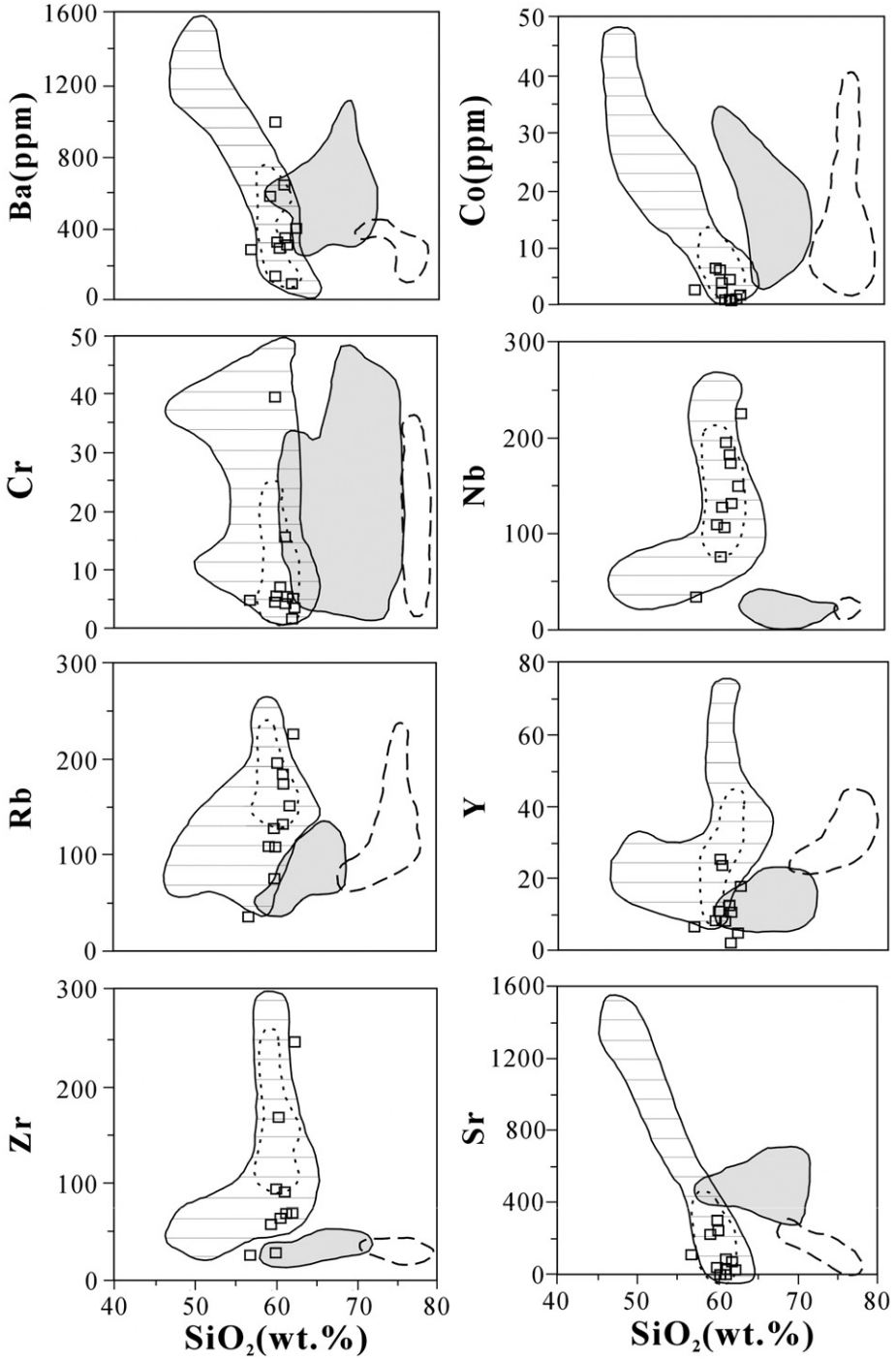

Fig. 6. Relationship between SiO_2 and trace elements for Ulleungdo monzonites. Symbols are the same as in Fig. 5.

In contrast to biotite and hornblende minerals, feldspar samples processed by crushing tend to have lower and variable $^3He/^4He$ ratios, ranging from 0.5 to 4 R_A. Three of six feldspar samples (U6, U11 and U12) show significantly higher $^3He/^4He$ ratios in the powder melting experiment compared to those processed by crushing, up to 30 R_A. These high ratios clearly indicate the presence of cosmogenic helium enriched in ^3He. If we assume that the original $^3He/^4He$ ratios of the feldspar samples were identical to those obtained by crushing, i.e., neglecting radiogenic contribution in the mineral lattice, surface exposure ages of U6, U11 and U12 samples are calculated to be 10.2 ± 1.6, 2.8 ± 1.2, and 12.8 ± 2.9 ka, respectively, adopting a production rate of cosmogenic ^3He of 100 ± 10 atoms/g/yr at this latitude (Yokochi et al., 2005). The maximum exposure age of ca. 10 ka is in broad agreement with the ^{14}C age of the U-4 tephra formation age (9.8–7.5 ka, Shiihara et al., 2004), in which the monzonites were carried to the surface. Since helium concentrations in all feldspar samples vary only by a factor of two, less significant differences in $^3He/^4He$ ratios between crushing and powder melting of the other feldspar samples indicate less cosmogenic contributions. This suggests that these samples had been buried in the tephra, because cosmogenic ^3He production rate decreases by an order of magnitude at the depth of 1 m below surface (Lal, 1987).

Those hornblende and biotite mineral separates from the samples that contain a significant cosmogenic contribution in feldspar, also show a slight enrichment in ^3He in the powder melt-processed splits. This is attributed to the relatively large initial concentration of helium in these mineral species. Yokochi et al. (2005) reported that a large

Table 5
Sr–Nd isotopic data for representative Ulleungdo monzonite clasts

Sample no.	U1	U5	U6	U6 (WR)	U6 (Fd)	U6 (Hb)	U6 (Bi)	U7	U8	U9 (WR)	U9 (Fd)	U9 (Hb)	U10	U12	U16	U18	J2
Rb (ppm)	174	118	128	128	84.8	87.2	467	108	150	226	251	37.3	183	108	195	251	140
Sr (ppm)	1.83	301	308	332	458	38.2	15.6	247	71.2	25.7	44.0	7.2	2.01	219	2.78	3.73	28.7
Rb/Sr	95.1	0.39	0.42	0.39	0.19	2.28	30.0	0.44	2.11	8.77	5.71	5.18	91.1	0.50	70.3	67.4	4.9
$^{87}Rb/^{86}Sr$	275	1.13	1.20	1.12	0.54	6.61	86.7	1.27	6.10	25.5	16.5	15.1	264	1.43	203	195	14.1
$^{87}Sr/^{86}Sr$	0.709898	0.704544	0.704848	0.704704	0.704701	0.704725	0.704840	0.705929	0.704894	0.704670	0.704672	0.704759	0.712641	0.704802	0.707285	0.707640	0.706619
±2σm		±17	±13	±16	±16	±16	±17	±14	±14	±16	±14	±17	±14	±17	±24	±17	±16
Sm (ppm)	3.09	3.82	4.77	14.26	0.54	45.8	10.33	1.69	1.98	3.08	1.30	23.1	1.78	2.11	3.30	6.62	1.59
Nd (ppm)	20.7	24.9	33.0	90.6	3.97	272	68.1	9.90	13.3	20.7	9.23	149	10.63	12.9	22.5	50.3	8.92
$^{147}Sm/^{144}Nd$	0.0902	0.0927	0.0873	0.0954	0.0822	0.1017	0.0914	0.1031	0.0899	0.0899	0.0851	0.0937	0.1015	0.0988	0.0886	0.0795	0.1077
$^{143}Nd/^{144}Nd$	0.512562	0.512560	0.512528	0.512528	0.512527	0.512526	0.512536	0.512566	0.512563	0.512559	0.512567	0.512567	0.512557	0.512577	0.512556	0.512552	0.512571
±2σm	±8	±8	±8	±7	±9	±8	±8	±8	±17	±8	±8	±7	±8	±10	±9	±8	±8
$\varepsilon Sr(t)^*$	61.7	0.51	4.91	2.78	2.81	2.91	0.11	20.2	5.21	1.03	1.52	2.86	101	4.19	28.6	34.0	29.3
$\varepsilon Nd(t)^*$	−1.48	−1.52	−2.14	−2.14	−2.16	−2.18	−1.99	−1.40	−1.46	−1.54	−1.38	−1.38	−1.58	−1.19	−1.60	−1.67	−1.30

$\varepsilon Sr(t)^*$ and $\varepsilon Nd(t)^*$ values were calculated at (0.27 Ma), using the following parameter: $^{87}Sr/^{86}Sr_{UR}=0.7045$, $^{87}Rb/^{86}Sr_{UR}=0.0827$, $\lambda^{87}Rb=1.42*10^{-11}y^{-1}$, $^{143}Nd/^{144}Nd_{CHUR}=0.512638$, $^{147}Sm/^{144}Nd_{CHUR}=0.1966$, $\lambda^{147}Sm=6.54*10^{-12}y^{-1}$ (Jacobsen and Wasserburg, 1980; Wasserburg et al., 1981). Rb, Sr, Sm and Nd concentrations were determined by the isotope dilution method. WR, whole rock; Fd, feldspar; Hb, hornblende., Bi, biotite. Numerals following isotopic ratios indicate uncertainties (2σm) corresponding to the last digit.

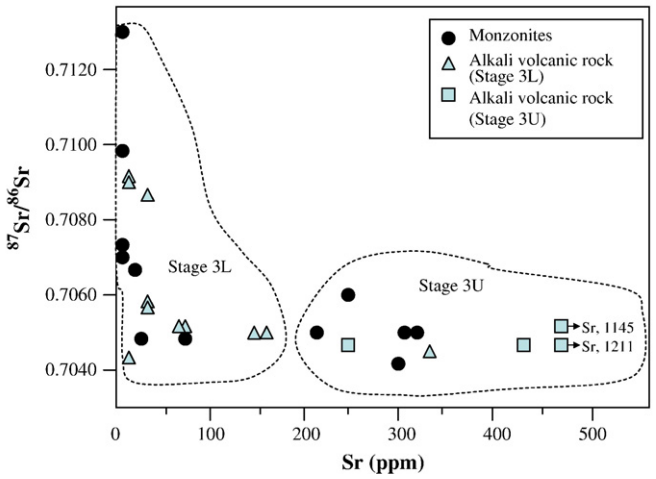

Fig. 7. Plot of Sr concentration versus $^{87}Sr/^{86}Sr$ ratios for Ulleungdo monzonites. Dotted areas indicate isotopic and Sr concentration for Ulleungdo Stage 3U and 3L alkali volcanic rocks (Kim et al., 1999).

number of crushing strokes actually heats the sample and/or induces fracturing in the lattice (defects) which then allows matrix-sited He to escape. However, the first and second crushing steps of U12 hornblende show identical $^{3}He/^{4}He$ ratios within analytical error, providing evidence that the radiogenic/cosmogenic component is not released even when 2000 strokes of crushing produces large surface areas exposed to cosmic rays. Although we have no constraint on possible production of radiogenic helium in minerals, due to the absence of mineral data for uranium and thorium concentrations, the fact that most samples plot above the 1:1 correlation line in Fig. 9 suggests that there is negligible contribution of the radiogenic component even during powder melting, except for U9-1 hornblende, which lies below the line.

5.2. Excess argon

Crush-released non-atmospheric ^{40}Ar ($^{40}Ar^*$) concentrations of the hornblendes can be calculated by the relationship $^{40}Ar^* = \{(^{40}Ar/^{36}Ar)_{measured} - (^{40}Ar/^{36}Ar)_{air}\} \times {}^{36}Ar$ (Table 6), are seen to roughly correlate with ^{4}He concentrations (Fig. 10). Note that the possible isotopic fractionation of argon inferred from $^{38}Ar/^{36}Ar$ ratio for some

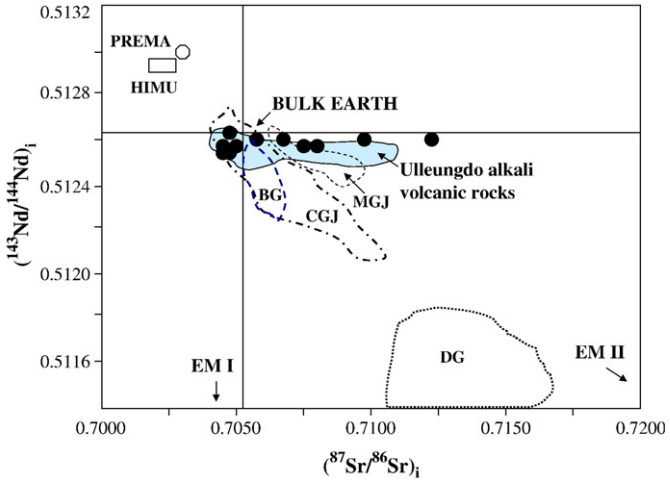

Fig. 8. Initial $^{87}Sr/^{86}Sr$ versus initial $^{143}Nd/^{144}Nd$ diagram for the Ulleungdo monzonites (closed circle). Ulleungdo alkali volcanic rocks (Kim et al., 1999). DG: Daebo granite, BG: Bulkuksa granite (Kim et al., 1996). MGJ and CGJ are the Japanese Miocene and Cretaceous granite samples (Terakado et al., 1988).

Table 6
Helium and argon isotopic compositions for late Pleistocene monzonite clasts from Ulleungdo volcanic island, South Korea

Sample	Mineral	Method	^{4}He	^{36}Ar	^{3}He/^{4}He (R_A)	^{38}Ar/^{36}Ar	^{40}Ar/^{36}Ar	^{40}Ar*	^{4}He/^{40}Ar*
U1	Hb	Crushing	5.43	0.018	5.86±0.10	0.18718±0.00072	378.5±1.2	1.50±0.15	3.62±0.51
		Powder melting	1.54	0.172	5.52±0.52	0.18838±0.00052	301.57±0.50	0.96±0.13	1.60±0.27
	Fd	Crushing	0.170	0.0204	0.5±1.3	0.18684±0.00077	744.9±3.1	9.16±0.92	0.0186±0.0026
		Powder melting	0.280	0.0735	2.03±0.61	0.18844±0.00055	312.75±0.47	1.23±0.13	0.227±0.033
U6	Hb	Crushing	56.1	0.158	6.03±0.13	0.18838±0.00041	368.72±0.40	11.5±1.2	4.87±0.69
		Powder melting	31.4	0.157	6.57±0.24	0.18702±0.00054	332.10±0.58	5.7±0.6	5.53±0.79
	Bi	Crushing	2.35	0.212	5.91±0.22	0.18841±0.00037	307.01±0.39	2.3±0.25	1.01±0.15
		Powder melting	4.15	0.217	6.48±0.19	0.18646±0.00044	310.51±0.38	3.1±0.33	1.32±0.19
	Fd	Crushing	0.290	0.057	1.09±0.79	0.18765±0.00052	438.40±0.48	8.2±0.8	0.0356±0.0050
		Powder melting	0.120	0.408	23.6±1.6	0.18693±0.00114	426.40±0.95	53.2±5.3	0.00226±0.00032
U9-1	Hb	Crushing	11.8	0.010	5.98±0.17	0.18676±0.00076	556.5±1.6	2.64±0.26	4.48±0.63
		Powder melting	5.7	0.142	4.34±0.16	0.18761±0.00082	303.47±0.50	1.06±0.13	5.40±0.84
	Fd	Crushing	0.180	0.0076	3.1±1.2	0.1856±0.0016	589.7±4.7	2.22±0.23	0.081±0.012
		Powder melting	0.160	0.0604	4.8±1.1	0.18810±0.00034	318.06±0.35	1.33±0.13	0.120±0.017
U10	Hb	Crushing	24.4	0.0125	6.15±0.12	0.18676±0.00058	806.5±1.6	6.39±0.64	3.82±0.54
		Powder melting	nd	0.0506	nd	0.18678±0.00045	299.60±0.60	0.18±0.04	
	Fd	Crushing	0.310	0.006	3.67±0.75	0.18500±0.00087	374.1±1.9	0.44±0.05	0.70±0.10
		Powder melting	0.400	0.175	2.78±0.50	0.18908±0.00061	304.00±0.38	1.40±0.15	0.286±0.043
U11	Hb	Crushing	9.9	0.031	6.37±0.11	0.18766±0.00048	481.37±0.82	5.7±0.6	1.73±0.25
		Powder melting	20.5	0.282	6.20±0.18	0.18891±0.00064	328.49±0.35	9.2±0.9	2.24±0.32
	Bi	Crushing	1.79	0.290	4.95±0.96	0.18687±0.00087	309.4±1.1	3.88±0.50	0.461±0.075
		Powder melting	1.20	0.323	5.97±0.57	0.18726±0.00070	305.59±0.52	3.10±0.35	0.387±0.059
	Fd	Crushing	0.110	0.082	4.0±1.2	0.18810±0.00057	1243.0±1.5	77.9±7.8	0.00141±0.00020
		Powder melting	0.190	0.245	7.9±1.0	0.18736±0.00074	452.5±2.2	38.4±3.9	0.00495±0.00070
U12	Hb	1st (1000 strokes)	2.34	0.00647	6.02±0.18	0.18686±0.00075	424.92±0.93	0.83±0.08	2.80±0.40
		2nd crush (1000 strokes)	0.37	0.00070	6.13±0.55	0.18735±0.00292	425.7±4.9	0.09±0.01	4.06±0.60
		Crush total	2.71	0.00717	6.03±0.17	0.18691±0.00073	425.00±0.96	0.92±0.08	2.93±0.40
		Powder melting	3.46	0.351	6.54±0.16	0.18576±0.00052	298.15±0.40	0.76±0.16	4.6±1.1
	Fd	Crushing	0.140	0.005	3.6±1.7	0.1866±0.0010	1111±19	4.44±0.46	0.0315±0.0046
		Powder melting	0.130	0.111	29.8±4.2	0.18825±0.00089	310.99±0.50	1.66±0.17	0.078±0.011
J1	Hb	Crushing	50.1	0.103	6.480±0.060	0.18800±0.00047	479.15±0.72	18.8±1.9	2.66±0.38
		Powder melting	48.5	0.063	6.41±0.16	0.18747±0.00039	388.39±0.78	5.8±0.6	8.3±1.2
	Bi	Crushing	2.71	0.311	6.07±0.24	0.18844±0.00036	308.40±0.29	3.85±0.40	0.70±0.10
		Powder melting	3.80	0.110	6.41±0.31	0.18833±0.00052	301.91±0.46	0.65±0.08	5.83±0.94

Unit of concentrations are 10^{-8} cm^{3}STP/g. Errors on ^{4}He and ^{36}Ar concentrations are 10%. Errors on isotope ratios are 1σ.
$^{40}Ar^* = \{(^{40}Ar/^{36}Ar)_{measured} - (^{40}Ar/^{36}Ar)_{air}\} \times {}^{36}Ar$. Hb: hornblende, Bi: biotite, Fd: feldspar. nd: not determined.

samples does not significantly affect calculated ^{40}Ar* beyond associated errors. This correlation apparently indicates that the ^{40}Ar* is excess argon trapped in fluid inclusions. The fact that the data obtained by powder melting of hornblende lies on the same trend suggests either that the majority of the derived ^{40}Ar* is dominated by contributions from undecrepitated fluid inclusions, or that the isotopic features of matrix-hosted helium and argon is similar to that in fluid inclusions. Feldspar samples deviate towards lower ^{4}He and/or higher ^{40}Ar* compared to the hornblende trend. Biotite samples also show a similar but smaller ^{4}He depletion and/or ^{40}Ar* enrichment. These can be explained either by (1) feldspar and biotite losing helium over geologic time while hornblende retained helium quantitatively; or (2) potassium contents in the three mineral species being generally in the order feldspar>biotite>hornblende, resulting in the observed isotopic differences in contributions of post-cooling radiogenic ^{40}Ar. Although we have no data on the density of fluid inclusions and noble gas concentrations in fluid inclusions in our minerals, we consider the first option to be more likely because amounts of ^{40}Ar* released by the powder melting are smaller than or similar to those released by the crushing extraction of the same sample (except U6 feldspar, which displays an anomalously large amount of ^{40}Ar* in the powder melting). Relatively low ^{3}He/^{4}He ratios in the crushed stage feldspars can be well explained by diffusive fractionation associated with preferential loss of helium (Harrison et al., 1999), as discussed later. Therefore, we conclude that the excess argon in the three mineral species was mostly trapped in fluid inclusions rather than in the crystal lattice.

In general, hornblende, biotite and feldspar are regarded as useful for K–Ar geochronology, because they display good argon retention properties (McDougall and Harrison, 1993). However, to reduce the effect of excess argon, we recommend separating measurements during crushing and heating steps, to separate excess argon in fluid inclusions from *in situ* argon produced in the crystal lattice after the cooling of the rock below the argon closure temperature, especially in the case of K–Ar dating of young samples.

5.3. Mantle helium in monzonite clasts from the back arc basin

Helium isotope characteristics for several back arc basins have been reported in detail by previous workers (e.g., Bach and Niedermann, 1993; Hilton et al., 1993; Macpherson et al., 1998; Sano et al., 1998; Marty et al., 2001). A compilation by Hilton et al. (2002) showed that back arc basins have lower ^{3}He/^{4}He ratios than those found in MORB, except for cases in which mantle-plume derived helium (with higher ^{3}He/^{4}He ratio than 8 R_A) is recognized. According to Hilton et al. (1993) and Shaw et al. (2006), several processes have the potential to influence the helium characteristics that are preserved in mineral phases: (1) *in situ* post-eruptive ingrowth; (2) addition of radiogenic helium with low ^{3}He/^{4}He of ca. 0.02 R_A associated with crustal assimilation (van Soest et al., 2002); (3) radiogenic ingrowth as a result of magma ageing (Zindler and Hart, 1986); and (4) diffusion-controlled isotopic fractionation (Harrison et al., 2004).

In the Ulleungdo monzonites, mantle helium was observed in hornblende (^{3}He/^{4}He ratios ranging from 5.9 to 6.5 R_A; only in crushed separates (see Fig. 11)). These values are in the range of back arc volcanics (Hilton et al., 2002) and of subcontinental lith1ospheric mantle (SCLM) (Gautheron and Moreira, 2002; Kim et al., 2005; Yamamoto et al., 2004). ^{4}He/^{40}Ar* ratios of 1.7–4.9 in hornblende from the Ulleungdo monzonites cover mantle production ratios (^{4}He/^{40}Ar* = 2–4), which are estimated from the mantle (U+Th)/K ratio (Allègre et al., 1986; Graham, 2002). Biotite samples show ^{3}He/^{4}He ratios almost identical to those of hornblende within analytical error,

Table 7
Ne, Kr and Xe isotopic compositions for late Pleistocene monzonite clasts from Ulleungdo volcanic island, South Korea

Sample No.	Mineral	Method	^{20}Ne	^{84}Kr	^{132}Xe	^{20}Ne/^{22}Ne	^{21}Ne/^{22}Ne
U1	Hb	Crushing	0.0638	0.0007	0.00008	9.97±0.05	0.02908±0.00041
		Powder melting	0.0122	0.0136	0.0360	10.00±0.07	0.0300±0.0015
	Fd	Crushing	0.0875	0.00044	0.00003	9.99±0.05	0.02938±0.00030
		Powder melting	0.0190	0.00746	0.00400	9.95±0.12	nd
U6	Hb	Crushing	0.121	0.00439	0.0003	9.87±0.04	0.02882±0.00022
		Powder melting	0.085	0.00788	0.0227	10.03±0.09	0.0296±0. 0035
	Bi	Crushing	0.0775	0.00615	0.000348	9.77±0.04	0.02905±0.00035
		Powder melting	0.0483	0.00904	0.000211	10.09±0.07	0.0313±0.0010
	Fd	Crushing	0.846	0.0188	0.0102	10.38±0.05	0.02963±0.00034
		Powder melting	0.588	0.0141	0.0081	10.20±0.03	0.02997±0.00041
U9-1	Hb	Crushing	0.0266	0.0005	0.0001	9.99±0.04	0.02916±0.00033
		Powder melting	0.0189	0.0166	0.0625	9.98±0.07	0.0310±0.0030
	Fd	Crushing	0.0196	0.0001	0.00001	10.11±0.08	0.02900±0.00030
		Powder melting	0.0075	0.0188	0.00789	9.84±0.07	0.02977±0.00087
U10	Hb	Crushing	0.0307	0.00031	0.00005	10.04±0.06	0.02952±0.00040
		Powder melting	0.0179	0.00433	0.00121	9.79±0.07	0.02883±0.00067
	Fd	Crushing	0.0193	0.0001	0.00001	10.06±0.04	0.02965±0.00068
		Powder melting	0.0047	0.0714	0.0191	9.96±0.08	0.0305±0.0015
U11	Hb	Crushing	0.0115	0.0009	0.00006	9.84±0.06	0.02921±0.00048
		Powder melting	0.0174	0.0458	0.0219	9.89±0.04	0.0301±0.0010
	Bi	Crushing	0.0002	0.0080	0.0005	10.35±0.29	0.0294±0.0012
		Powder melting	0.0275	0.0146	0.0264	9.86±0.04	0.03182±0.00033
	Fd	Crushing	0.0225	0.00386	0.000253	10.17±0.07	0.03132±0.00046
		Powder melting	0.0099	0.00719	0.000711	9.75±0.03	0.02952±0.00047
U12	Hb	Crushing	0.0061	0.00024	0.000020	9.823±0.069	0.02945±0.00065
		Powder melting	0.0418	0.0108	0.00572	10.14±0.07	0.0296±0.0017
	Fd	Crushing	0.00541	0.0001	0.00001	9.99±0.11	0.02999±0.00095
		Powder melting	0.00860	0.0201	0.00651	9.87±0.03	0.03057±0.00076
J1	Hb	Crushing	0.0250	0.00334	0.00021	9.89±0.05	0.02998±0.00034
		Powder melting	0.0283	0.00304	0.00486	9.82±0.04	0.03009±0.00052
	Bi	Crushing	0.0890	0.00880	0.00045	9.79±0.05	0.02906±0.00034
		Powder melting	0.0099	0.00234	0.00488	9.72±0.03	0.02878±0.00046

Unit of concentrations are 10^{-8}cm^{3}STP/g. Errors on noble gas concentrations are 10%. Errors on isotope ratios are 1σ.
Hb: hornblende, Bi: biotite, Fd: feldspar. nd: not determined.

but with distinctively low ^{4}He/^{40}Ar* ratios. Feldspar samples possess much lower ^{3}He/^{4}He and ^{4}He/^{40}Ar* ratios. Most data for biotite and feldspar samples are in broad agreement with the theoretical diffusive fractionation model of Harrison et al. (2004), assuming initial ^{3}He/^{4}He and ^{4}He/^{40}Ar* ratios are 6.2 R_A (an average ^{3}He/^{4}He ratio for hornblende) and 6, respectively (Fig. 11). A lower initial ^{4}He/^{40}Ar* ratio down to 2, based upon a range observed in hornblende samples, does not change the discussion. The agreement indicates that hornblende can preserve helium, while some helium in biotite, and most helium in feldspar, is rapidly lost during or after cooling. This

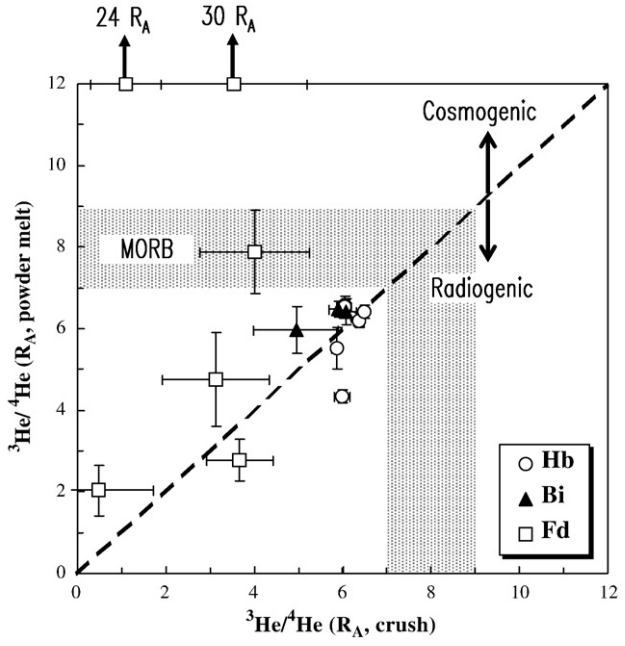

Fig. 9. A correlation diagram of ^{3}He/^{4}He ratios of mineral separates from Ulleungdo monzonites obtained with via crushing and powder melting. The dashed line gives the 1:1 correlation line. Error bars are 1σ. Hb, Bi, and Fd are hornblende, biotite, and feldspar, respectively. The effects of cosmogenic and radiogenic addition to isotopic ratios are shown by arrows. The hatched area indicates the ^{3}He/^{4}He ratio of MORB source mantle (8±1 R_A).

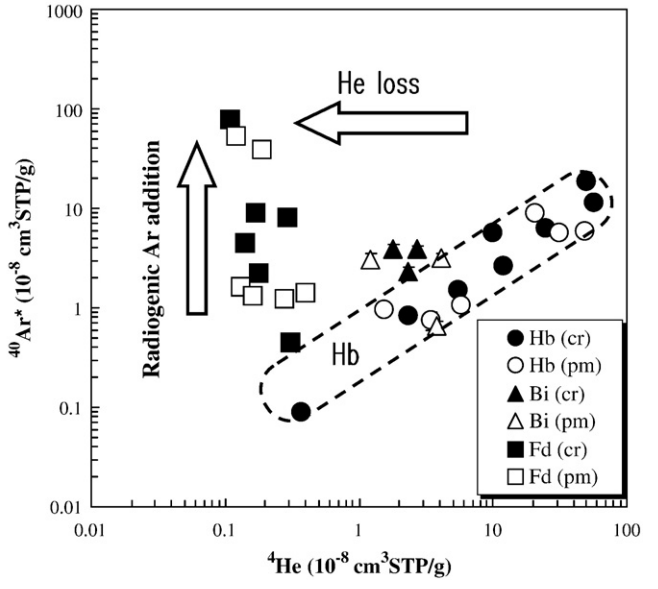

Fig. 10. ^{4}He– ^{40}Ar* relationships for mineral separates from the Ulleungdo monzonites. Filled and closed symbols are obtained with the crushing (cr) and powder melting (pm) methods, respectively.

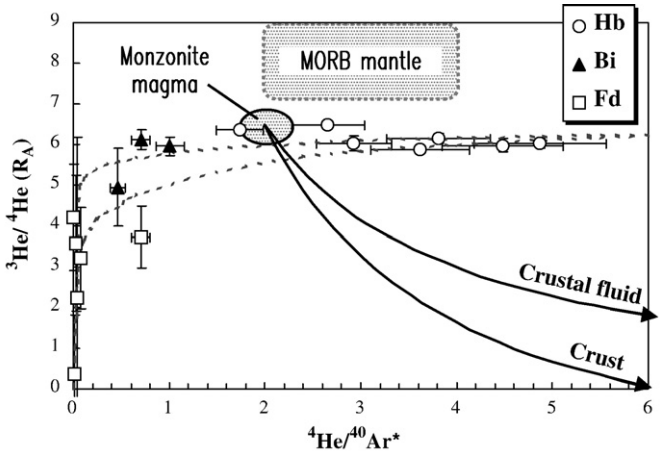

Fig. 11. Correlation between ^{3}He/^{4}He and ^{4}He/^{40}Ar* ratios of mineral separates from the Ulleungdo monzonites obtained with the crushing extraction method. Errors are 1σ. Hatched areas indicate the ^{3}He/^{4}He ratio of MORB source mantle. Two dotted lines are theoretical diffusive fractionation lines assuming initial ^{3}He/^{4}He and ^{4}He/^{40}Ar* ratios of 6.2 R$_A$ and 6, with ^{3}He diffusivity higher than that of ^{4}He by 5% and 15% [Harrison et al., 2004]. Two solid lines are mixing trends of a single monzonite parental magma with crustal material and crustal fluid (see text).

concurs with experimental results dealing with the helium retention behavior of hornblende, sanidine and muscovite (Lippolt and Weigel, 1988). Similarity of the maximum cosmogenic ^{3}He exposure age of the feldspar separates, and the eruption age, indicates that the helium loss occurred neither after the eruption nor during sample treatment and/or baking in vacuum prior to the noble gas analysis. Therefore, the helium depletion in biotite and feldspar must result from slow cooling and storage of the monzonites in the depths and/or heating by host magma during transport of the monzonites to the surface, leading to subsequent volatile loss by diffusion from fluid inclusions.

As mentioned above, neon isotopes and ^{38}Ar/^{36}Ar ratios are also fractionated (Tables 6 and 7). However, their fractionation trends of light isotope enrichment are contrary to the helium loss, and are observed not only in feldspar and biotite but also in hornblende. It is not clear whether the fractionated atmosphere-like feature is germane to the monzonites, or whether it is an atmospheric contaminant. Further study will test the idea that He is in fact lost by diffusion.

Two hornblende samples (U11 and J1) have slightly higher ^{3}He/^{4}He and lower ^{4}He/^{40}Ar* than the main hornblende population (Fig. 11). This trend cannot be explained by diffusive fractionation. In the case of the Ulleungdo monzonites, because of their extremely young eruption age less than 10 ka (Shiihara et al., 2004) post-eruptive ingrowth of radiogenic ^{4}He is insufficient to produce these low ^{3}He/^{4}He values. Moreover, the crushing extraction method minimizes a contribution of this component. Therefore, ^{3}He/^{4}He and ^{4}He/^{40}Ar* differences amongst the hornblendes may reflect radiogenic ingrowth or progressive crustal contamination of the felsic magma during its storage at depth. Since these two processes decrease ^{3}He/^{4}He values, the original isotopic composition of the source monzonite magma must have been ^{3}He/^{4}He > 6.5 R$_A$ and ^{4}He/^{40}Ar* < 2, assuming the that all monzonites were derived from a single parental magma. However, a possible mixing line between the magmatic and crustal component (^{3}He/^{4}He = 0.02 R$_A$ and ^{4}He/^{40}Ar* = 6: production ratios in the average crust, Andrews, 1985; Ballentine et al., 1994) and the magmatic component and ^{4}He-enriched crustal fluid with ^{4}He/^{40}Ar* ratios up to 25 (Ballentine et al., 1994), cannot explain the sample trend.

We have no strong control on the period of time that elapsed during cooling to the point that helium began to be retained in hornblende, or uranium and thorium concentrations for monzonite magma. However, it is suggested that source magma of the monzonites was cogenetically evolved from Stage 3 trachytic magma that produced Ulleungdo alkali volcanism. Actually, K_2O contents of the monzonites (6.0–7.0 wt.%) are similar to those of the Stage 3 trachytes (4.5–6.6 wt.%, Kim et al., 1999); other major compositional similarities are also evident. Assuming a thorium content of the monzonite magma to have been 21 ppm (average for Stage 3 trachyte, Kim et al., 1999) with a Th/U ratio of 3, the estimated ^{4}He/^{40}Ar* production ratio was 5.7, resulting in an isotopic evolution line much the same as the magma-crust mixing line in Fig. 11.

Therefore, we consider that these processes would not be able to explain the ^{3}He/^{4}He and ^{4}He/^{40}Ar* variation of hornblende. A remaining possibility is mixing of magma with another component possessing ^{3}He/^{4}He values lower than 6 R$_A$ and ^{4}He/^{40}Ar* higher than 5. This includes the possibility that the higher ^{4}He/^{40}Ar* end of the hornblende trend itself is an end member. Alternatively, each monzonite clast might be derived from different source magmas, each bearing different ^{3}He/^{4}He and ^{4}He/^{40}Ar* ratios. We have no means of discriminating these possibilities at present; hence further investigation is required to clarify the origin of the He–Ar variation of the Ulleungdo monzonites.

As mentioned above, the ^{3}He/^{4}He ratio of the source magma of the monzonites is estimated to be higher than 6.5 R$_A$. Kim et al. (2005) reported that several low ^{3}He/^{4}He components, down to 0.2 R$_A$, with ^{4}He/^{40}Ar* ratios similar to that of MORB source mantle, are present in SCLM beneath the Korean Peninsula. They attribute these to the high time-integrated (U+Th)/^{3}He ratio of the metasomatized mantle wedge of an ancient subduction zone (Yamamoto et al., 2004; Kim et al., 2005). Hence, one would expect the original ^{3}He/^{4}He ratio of a magma source in SCLM to be around 6.5 R$_A$. On the other hand, clear contamination of seawater and crustal material has been recognized in the monzonites and the Stage 3 trachytes when they are compared to Stage 1 basalt of the Ulleungdo volcanics (Kim et al., 1999). Additionally, ^{3}He/^{4}He ratios close to the MORB value have also been reported for mantle-derived xenoliths from surrounding areas of the back arc basin (Kim et al., 2005; Nagao and Takahashi, 1993; Sumino et al., 2000; Yokochi et al., 2005). These lines of evidence suggest that the Ulleungdo magma assimilated continental crustal material, resulting in a low ^{3}He/^{4}He source within the back arc basin.

Both scenarios are possible at present. However, in any case, mantle-derived helium is dominant (more than 80%) in the monzonite source. A majority of excess argon is also of mantle origin because ^{4}He/^{40}Ar* ratios of mantle and crustal components are different by a factor of only two. Since the Ulleungdo monzonite is genetically linked to alkali volcanic rocks of the Ulleungdo, our helium isotope data provide strong direct evidence that the Ulleungdo felsic magma is mantle derived, which was one of the important debates concerning the origin of felsic and alkali basaltic magma in the back arc basin.

5.4. Volcano-plutonic magmatism in the back arc basin

Several different and debatable genetic models for the origin of the Ulleungdo alkali basaltic magma in relation to tectonic evolution in a back arc basin have been proposed that might also explain the origin of the felsic (monzonitic) magma. The models are as follows; (1) that the magma is a product of interaction between a mantle MORB source and a mantle plume (e.g., Morris and Kagami, 1989; Nakamura et al., 1990); (2) that the magma was originated from metasomatized subcontinental lithospheric mantle (e.g., Tatsumoto and Nakamura, 1991; Terakado et al., 1997; Shuto et al., 2004;); (3) that the magma is mantle mantle-derived basaltic magma contaminated by continental crustal materials (e.g., Kaneoka, 1990; Kim et al., 1999); (4) and that the magma is originated in the shallow asthenosphere, largely in response to drastic changes in stress regimes (e.g., Choi et al., 2006).

Continental fragments and rifted continent crustal blocks in a back arc basin has have been reported by Tamaki (1988). However, until now there was lack of any information on plutonic activities in this area. This finding of the Ulleungdo felsic plutonic rocks can give us an

important constraint for origin and evolution of alkali basaltic magma as well as presence of felsic (granitic) magma in the alkali volcanic province.

Three plausible candidates for the source material of the felsic (monzonitic) rocks in the Ulleungdo tephra formation of Paleogene age can be considered. Firstly, the same source as the Jurassic Daebo and Cretaceous Bulguksa granites, which are widely distributed in the inland of the Korean peninsula and in a back arc basin as remnant continental blocks on the sea floor of the East Sea and the Japan Sea. And Cretaceous and Neogene granites in the Japanese island may also have the same source. However, the unique young ages for the Ulleungdo felsic plutonic rocks revealed by our radiometric dating can conclusively eliminate above source candidate that of Mesozoic Daebo and Cenozoic Bulguksa granites already identified in the back arc basin by a previous drilling survey (Tamaki, 1988).

Secondly, an alternative assumption that pre-existing continental protoliths such as Jurassic and Cretaceous granites beneath the Ulleungdo volcanic island may have been isotopically reset during the evolution of Ulleungdo's Pleistocene alkali volcanic activities. This hypothesis does not explain the similar chemical and isotopic compositions of the Ulleungdo monzonitic rocks and the alkali volcanic rocks. The excess argon observed in hornblende minerals as shown by the K–Ar isotopic data (Fig. 3) and Ar–Ar age spectrum (Fig. 4). Excess argon in fluid inclusions in hornblende was identified by *in vacuo* crushing and heating (1800 °C) extraction experiment to distinguish the trapped magmatic component, and radiogenic and cosmogenic isotopes remain close to their production sites within the crystal lattice. For example, hornblende sample (U10) shows a significant isotopic difference between two sources of argon such as fluid inclusion argon ($^{40}Ar/^{36}Ar=806.5$) and crystal lattice argon ($^{40}Ar/^{36}Ar=299.6$), suggesting the presence of excess argon in fluid inclusion. The isotopic ratios of crystal lattice argon ($^{40}Ar/^{36}Ar=299.6$) yield the extremely young age, corresponding to the Rb–Sr isochron and K–Ar ages. Our results are consistent to widely accepted view that hornblende displayed good Ar retention properties even at the high temperature. In addition to the geochemical and isotopic similarities, the similar formation and eruption ages for the monzonites (0.12–0.29 Ma) and the trachytic volcanics of substage 3U (0.24–0.47 Ma) suggest that the felsic magma may have evolved from the Stage 3 trachytic magma. It also strongly suggests that the monzonites are interpreted as cumulate rocks from, and intrusive equivalent of, fractionated trachytic magma. In Figs. 5, 6 and 8, the geochemical and Nd–Sr isotopic data for the Ulleungdo monzonites are clearly plotted overlapping the compositions of the Stage 3 alkali volcanic rocks.

One possible interpretation of our geochemical data is that a small volume of felsic magma was formed by *in situ* fractional crystallization of trachytic magma of Stage 3 which evolved from the parent alkali basaltic magma of Stage 1 in the open system of the magma chamber beneath the Ulleungdo volcano. Occurrence of basalt inclusions in trachyte body of the 3U substage provides a strong support for the above interpretation. In terms of occurrence, geochemistry and Sr isotopic signatures, the Ulleungdo felsic plutonic rocks are analogous to those from Ascension Island, South Atlantic Ocean (Kar et al., 1998). However, no cumulus fabrics are observed in the Ulleungdo monzonites. In general, oceanic island felsic volcanism is typically interpreted as the product of fractional crystallization of mafic magma derived from hot spot related plume sources (e.g., Storey et al., 1989; Zellmer et al., 2005). In the case of the Ulleungdo monzonites, the mantle source helium with a $^3He/^4He$ ratio of 5.9–6.5 R_A, which falls in range between 3.5 and 7.9 R_A of mantle xenoliths in the Korean peninsula (Kim et al., 2005), was identified from hornblende samples which are interpreted as a source of lithospheric mantle. However, Terakado et al. (1988) reported that the typical MORB-like materials were not directly involved in the formation of igneous rocks in the back arc basin during the opening the Japan Sea.

Generation of alkali basaltic magmatism at Ulleungdo would have begun between 1.37 and 0.97 Ma during the development of the back arc basin (Kim et al., 1999). Isotopic evidence suggests the basalts were generated from a metasomatized old subcontinental mantle wedge source (Kim et al., 2005). Major and trace element data indicates that trachytic rocks were then differentiated from the alkali basaltic magma by fractional crystallization (Kim, 1985; Kim et al., 1999). The incorporation of crustal materials and ambient seawater significantly enhanced strontium isotopic values during the early stage of volcanism (1.37–0.77 Ma) (Fig. 12A). During Stage 3 of volcanic activity (0.73–0.24 Ma), the voluminous crustal contaminated trachytic rocks of substage 3L and 3U were extruded (Fig. 12B). Substage 3L trachytes show high initial $^{87}Sr/^{86}Sr$ and Rb/Sr ratios, while trachytes from substage 3U have low $^{87}Sr/^{86}Sr$ and Rb/Sr ratios (Fig. 12B). This difference is probably caused by different levels of crustal assimilation in the magma chamber. As shown in Fig. 7, it is interesting to note that young monzonitic rocks bear similar chemical and Sr isotopic characteristics to trachytic rocks of substage 3L and 3U (Fig. 12C),

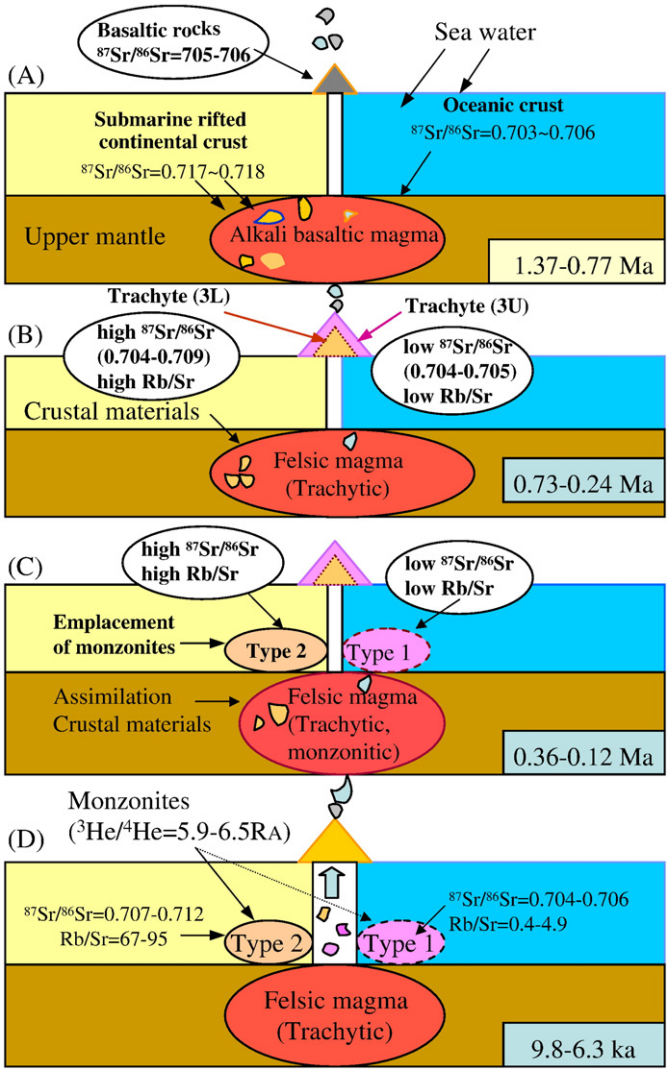

Fig. 12. A schematic representation of the evolution of felsic magma at Ulleungdo. (A) Incorporation of crustal material and coeval seawater in the alkali basaltic magma (1.37–0.77 Ma). (B) Eruption of felsic (trachytic) magma that evolved from the alkali basaltic magma. Trachytic rocks can be divided into two substages, 3L and 3U, which have different Sr concentrations and isotopic ratios. (C) Subsurface solidification of felsic (monzonitic) magma (0.36–0.12 Ma), which evolved from the primary alkali basaltic magma via trachytic magma near the volcanic vent, and (D) Plinian style eruption of high viscosity trachytic magma containing lots of monzonite blocks (9.8–6.3 ka). Strontium isotopic data are from Kim et al. (1999).

implying that similar magmatic processes occurred in the formation of trachytic and monzonitic magmas despite the different magmatic stage. The high $^{87}Sr/^{86}Sr$ and Rb/Sr ratios of Type 2 monzonites suggest that the origin of Stage 3 trachytic magma was from minor fractional crystallization of mafic magma coupled with large-scale assimilation of old continental crust with high $^{87}Sr/^{86}Sr$ ratios preserved in the back arc basin. Meanwhile, the low $^{87}Sr/^{86}Sr$ and Rb/Sr ratios of Type 1 monzonites indicate that trachytic magma formed by limited crustal contamination and/or assimilation of mantle mantle-derived oceanic crustal materials with low $^{87}Sr/^{86}Sr$ ratios during magmatic differentiation. Ulleungdo monzonites are intrusive equivalents of the fractionating felsic magma (monzonitic or trachytic) that also produced the trachytic volcanic rocks. At 0.2–0.1 Ma, comparatively small monzonite plutons containing mantle helium, were emplaced near the central volcanic vent. These plutons crystallized from rejuvenated felsic magma, which had formed by similar magmatic processes to those of the Stage 3 trachytic magma (Fig. 12C). However, no coherent geochemical evidence of *in situ* fractional crystallization has been found, suggesting that the fractionating trachytic magma underwent heterogeneous crustal assimilation. In the next stage of volcanism (9.8–6.3 ka), the Plinian style of eruption caused the collapse of the volcanic vent producing voluminous tephras containing a small volume of monzonitic blocks as accessory lithics (Fig. 12D).

We conclude that the Ulleungdo monzonites evolved from Stage 1 alkali basaltic magma via trachytic magma of Stage 3 by *in situ* fractional crystallization with an extremely short incubation time of less than 0.12 Myr in the Ulleungdo volcano. Elemental variations also support the fractional crystallization. Assimilation of crustal materials may possibly play an important role in changing the magmatic fluids from alkali basaltic to trachytic or felsic magma.

This represents important fresh *in situ* evidence of the formation of exceptionally young new felsic plutonic rocks in the magma chamber of the extensional tectonic zone of the back arc basin of an alkali volcanic province. The pronounced gravity heights and magnetic anomaly patterns around the Ulleung basin, suggesting the presence of felsic bodies beneath the basin (Han et al., 1997) also support the new sizable felsic plutonic rocks in the Ulleungdo volcano. Extremely young ages for monzonites in the Ulleungdo also suggest that the plutonic activities beneath the back arc basin are linked to an opening of the East Sea and the Japan Sea. Such activity might be induced by mantle upwelling behind the Japanese island arc of the southeastern active continental margin of the Eurasian plate (Iwamori, 1991). The Ulleungdo volcanic island also provides us with an excellent place to investigate the temporal and spatial relationship between volcanic and plutonic magmatism occurring *in situ* close to real time.

6. Conclusions

We observed that plutonic silicate minerals such as hornblende (and to lesser extents biotite) are useful for noble gas analysis in order to gain insight into magmatic processes in a volcano-plutonic magmatic system of the Japanese back arc basin. This is because these minerals can trap mantle volatiles within fluid inclusions during crystallization. On the other hand, volatiles trapped in feldspar minerals preferentially lose most helium during cooling and storage of the monzonites at depth and/or during transportation of the monzonites to the surface in a hot host magma.

A mantle helium component ($^3He/^4He$ of ca. 6 R_A, $^4He/^{40}Ar^*$=2–5) was found in plutonic silicate phases such as hornblende of the late Pleistocene Ulleungdo monzonites. The fact that the $^3He/^4He$ ratio of the Ulleungdo monzonites is more radiogenic than MORB source mantle implies that the Ulleungdo felsic magma might have (1) originated from metasomatized SCLM by subduction-related process within the continental margin of the southeastern end of the Eurasian plate, as suggested by noble gas studies of mantle xenoliths of this region; or (2) that magma derived from MORB-type mantle was contaminated by a crustal component during magma differentiation, as revealed by Nd–Sr isotopic studies of the Ulleungdo monzonites and alkali volcanic rocks.

Significant excess argon was found in fluid inclusions in three mineral species (hornblende, biotite and feldspar), which are generally regarded as good minerals to use to obtain K–Ar ages of plutonic rocks. This indicates that a combination of crushing and heating extraction methods, and comprehensive noble gas isotope measurements to separate excess argon, are especially useful for K–Ar dating of young samples. Our discovery of mantle helium and argon in the Ulleungdo monzonites may be applied to other young Pleistocene plutonic rocks from around the world.

He–Ar and Nd–Sr isotopic signatures together with the radiometric ages and geochemical characteristics of the Ulleungdo monzonites strongly suggest that the felsic (monzonitic) magma was cogenetically evolved from alkali basaltic magma via fractionating felsic trachytic magma, formed in the back arc basin and related to the opening of the East Sea and the Japan Sea.

Acknowledgments

This work was supported by a Korean Research Foundation Grant (KRF-2005-013-C0041) and COPRI project (PP08030) in part to Kyu Han Kim and Jong Ik Lee. We are very grateful to M. Okuno for their help with the sample collection. We thank the members of the Radioisotope Center, University of Tokyo and Irradiation Experiment Facilities, Institute for Materials Research, Tohoku University for providing experimental facilities and the neutron irradiation at the Japan Materials Testing Reactor. We also thank D. R. Hilton, S. Niedermann, C. R. Bacon and an anonymous reviewer for providing thorough constructive reviews that significantly improved the manuscript.

References

Allègre, C.J., Staudacher, Th., Sarda, P., 1986. Rare gas systematics: formation of atmosphere, evolution and structure of Earth s mantle. Earth Planet. Sci. Lett. 87, 127–150.
Andrews, J.N., 1985. The isotopic composition of radiogenic helium and its use to study groundwater movement in confined aquifers. Chem. Geol. 49, 339–351.
Bach, W., Niedermann, S., 1993. Atmospheric noble gases in volcanic glasses from the southern Lau Basin: origin from the subducting slab? Earth Planet. Sci. Lett. 160, 297–309.
Bacon, C.R., Lowenstern, J.B., 2005. Late Pleistocene granodiorite source for recycled zircon and phenocrysts in rhyodacite lava at Crater Lake, Oregon. Earth Planet. Sci. Lett. 233, 277–293.
Bacon, C.R., Persing, H.M., Wooden, J.L., Ireland, T.R., 2000. Late Pleistocene granodiorite beneath Crater Lake caldera, Oregon, dated by ion microprobe. Geology 28, 467–470.
Ballentine, C.J., Mazurek, M., Gautschi, A., 1994. Thermal constraints on crustal rare gas release and migration: evidence from Alpine fluid inclusions. Geochim. Cosmochim. Acta 58, 4333–4348.
Bohrson, W.A., Reid, M.R., 1997. Genesis of silicic peralkaline volcanic rocks in an ocean island setting by crustal melting and open system processes, Socorro Island, Mexico. J. Petrol. 38, 1137–1166.
Bonin, B., Bebien, J., 2005. The granite-upper mantle connection in terrestrial planetary bodies: an anomaly to the current granite paradigm? Lithos 80, 131–145.
Charier, B.I.A., Wilson, C.J.N., Lowenstern, J.B., Blake, S., Van Calsteren, P.W., Davidson, J.P., 2005. Magma generation at a large, hyperactive silicic volcano (Taupo, New Zealand) Revealed by U–Th and U–Pb systematics in zircons. J. Petrol. 46, 3–32.
Choi, S.H., Mukasa, S.B., Kwon, S., Andronikov, A.V., 2006. Sr, Nd, Pb and Hf isotopic compositions of late Cenozoic alkali basalts in South Korea: evidence for mixing between the two dominant asthenospheric mantle domains beneath East Asia. Chem. Geol. 232, 134–151.
Dalrymple, G.B., Grove, M., Lovera, O.M., Harrison, T.M., Hulen, J.B., Lanphere, M.A., 1999. Age and thermal history of the Geysers plutonic complex (felsic unit), Geysers geothermal field, California: a $^{40}Ar/^{39}Ar$ and U–Pb study. Earth PlenetPlanet. Sci. Lett. 173, 285–298.
Dini, A., Gianelli, G., Puxeddu, M., Ruggieri, G., 2005. Origin and evolution of Pliocene–Pleistocene granites from the Larderello geothermal field (Tuscan Magmatic Province, Italy). Lithos 81, 1–31.
Dufek, J., Bergantz, G.W., 2005. Lower crustal magma genesis and preservation: a stochastic framework for the evaluation of basalt–crust interaction. J. Petrol. 46, 2167–2195.
Ebisawa, N., Sumino, H., Okazaki, R., Takigami, Y., Hirano, N., Nagao, K., Kaneoka, I., 2004. Construction of I–Xe and $^{40}Ar–^{39}Ar$ dating system using a modified VG3600 mass spectrometer and the first I–Xe data obtained in Japan. J. Mass Spectrom. Soc. Jpn. 52, 219–229.

Eby, G.N., 1990. The A-type granitoids: a review of their occurrence and chemical characteristics and speculations on their genesis. Lithos 26, 115–134.
Gautheron, C., Moreira, M., 2002. Helium signature of the subcontinental lithospheric mantle. Earth Planet. Sci. Lett. 199, 39–47.
Graham, D.W., 2002. Noble gas isotope geochemistry of Mid-ocean ridge and ocean island basalts: characterization of mantle source reservoirs. Rev. Mineral. Geochem. 47, 247–317.
Han, S.J., Kim, H.J., Huh, S., Park, C.H., Kim, S.R., Lee, Y.K., Yoo, H.S., Choi, D.I., Park, B.K., 1997. Basin structure of the northeastern Ulleung basin (Ulleung and Dok island areas), East Sea of Korea. J. Geol. Soc. Korea 33, 127–138 (in Korean with English abstract).
Harayama, S., 1990. Geology of the Kamikochi district: Geological Survey of Japan, scale 1:50,000, p.175 text (in Japanese with English abstract).
Harayama, S., 1992. Youngest exposed granitoid pluton on Earth: cooling and rapid uplift of the Pleiocene–Quaternary Takidani granodiorite in the Japan Alps, Central Japan. Geology 20, 657–660.
Harrison, D., Burnard, P., Turner, G., 1999. Noble gas behaviour and composition in the mantle: constraints from the Iceland Plume. Earth Planet. Sci. Lett. 171, 199–207.
Harrison, D., Barry, T., Turner, G., 2004. Possible diffusive fractionation of helium isotopes in olivine and clinopyroxene phenocrysts. Eur. J. Mineral. 16, 213–220.
Hilton, D.R., Hammerschmidt, K., Loock, G., Friedrichsen, H., 1993. Helium and argon isotope systematics of the central Lau Basin and Valu Fa ridge. Geochim. Cosmochim. Acta 57, 2819–2841.
Hilton, D.R., Fischer, T.P., Marty, B., 2002. Noble gases and volatile recycling at subduction zones. Rev. Mineral Geochem. 47, 319–370.
Iwamori, H., 1991. Zonal structure of Cenozoic basalts related to mantle upwelling in southwest Japan. J. Geophys. Res. 96, 6157–6170.
Kaneoka, I., 1980. Rare gas isotopes and mass fractionation: an indicator of gas transport into or from magma. Earth Planet. Sci. Lett. 48, 284–292.
Kaneoka, I., 1990. Radiometric age and Sr isotope characteristics of volcanic rocks from the Japan Sea floor. Geochem. J. 24, 7–19.
Kar, A., Weaver, B., Davidson, J., Colucci, M., 1998. Origin of differentiation volcanic and plutonic rocks from Ascension Island, South Atlantic Ocean. J. Petrol. 39, 1009–1024.
Kelemen, P.B., Hanghoj, K., Greene, A.R., 2004. One view of the geochemistry of subduction-related magmatic arcs, with an emphasis on primitive andesite and lower crust. In: Roberta, L.R., Holland, H.D., Turekian, K.K. (Eds.), Treatise on Geochemistry, vol. 3. Elsevier, pp. 593–659.
Kim, Y.K., 1985. Petrology of Ulreung island, Korea. Part 2, Petrography and bulk chemical composition. J. Min. Petr. Econ. Geol. 80, 292–303 (in Japanese with English abstract).
Kim, K.H., 1992. Geochemical study of some Mesozoic granitic rocks in South Korea. J. Korean Inst. Mining Geol. 25, 435–446 (in Korean with English abstract).
Kim, K.H., Park, S.S., Na, C.K., 1996. Nd and Sr isotopic signatures of Mesozoic granitoids in South Korea. Resource Geology 46, 215–226.
Kim, K.H., Tanaka, T., Nagao, K., Jang, S.K., 1999. Nd and Sr isotopes and K–Ar ages of Ulreungdo alkali volcanic rocks in the East Sea, South Korea. Geochem. J. 33, 317–341.
Kim, K.H., Nagao, K., Tanaka, T., Sumino, H., Nakamura, T., Okuno, M., Lock, J.B., Youn, J.S., Song, J., 2005. He–Ar and Nd–Sr isotopic compositions of ultramafic xenoliths and host alkali basalts from the Korean peninsula. Geochem. J. 39, 341–356.
Kurasawa, H., Imanaga, I., Matsumoto, A., Shibata, K., 1989. K–Ar age and chemical and strontium isotopic compositions of the Yaguradake quartz diorite, Ashigara, Central Japan. J. Geol. Soc. Japan 9, 331–334 (in Japanese with English abstract).
Kurz, M.D., 1986. Cosmogenic helium in a terrestrial igneous rock. Nature 320, 435–439.
Jacobsen, S.B., Wasserburg, G.J., 1980. Sm–Nd isotopic evolution of chondrites. Earth Planet. Sci. Lett. 50, 139–155.
Lal, D., 1987. Production of ^{3}He in terrestrial rocks. Chem. Geol. 66, 89–98.
Le Maitre, R.W., Bateman, P., Dudek, A., Keller, J., Le Bas, M.J., Sabine, P.A., Schmid, R., Soresen, H., Streckeisen, A., Woolley, A.R., Zanettin, B., 1989. A Classification of Igneous Rocks and Glossary of Terms. Blackwell, Oxford.
Lipman, P.W., Bogatikov, O.A., Tsvetkov, A.A., Gazis, C., Gurbanov, A.G., Hon, K., Koronovsky, N.V., Kovalenko, V.I., Marchev, P., 1993. 2.8-Ma ash- flow caldera at Chegem River in the northern Caucasus Mountains (Russia), contemporaneous granites, and associated ore deposits. J. Volcanol. Geotherm. Res. 57, 85–124.
Lippolt, H., Weigel, E., 1988. ^{4}He diffusion in ^{40}Ar-retentive minerals. Geochim. Cosmochim. Acta 52, 1449–1458.
Lowenstern, J.B., Persing, H.M., Wooden, J.L., Lanphere, M., Donnelly-Nolan, J., Grove, T.L., 2000. U–Th dating of single zircons from young granitoid xenoliths: new tools for understanding volcanic processes. Earth Planet. Sci. Lett. 183, 291–302.
Ludwig, K.R., 1991. ISOPLOT: A Plotting and Regression Program for Radio-isotope Data, U.S. Geol. Survey Open-file Report 91-445. 39 pp.
Macpherson, C.G., Hilton, D.R., Sinton, J.M., Poreda, R.J., Craig, H., 1998. High ^{3}He/^{4}He ratios in the Manus back arc basin. Geology 26, 1007–1010.
Mamyrin, B.A., Anufriev, G.S., Kamensky, I.L., Tolstikhin, I.N., 1970. Determination of the isotopic composition of atmospheric helium. Geochem. Int. 7, 498–505.
Marty, B., Sano, Y., France-Lanord, C., 2001. Water saturated ocean lavas from the Manus Basin: volatile behavior during assimilation–fractional crystallization-degassing (AFCD). J. Volcanol. Geotherm. Res. 108, 1–10.
Matsuda, J., Matsumoto, T., Sumino, H., Nagao, K., Yamamoto, J., Miura, Y.N., Kaneoka, I., Takahata, N., Sano, Y., 2002. The ^{3}He/^{4}He ratio of the new internal He standard of Japan (HESJ). Geochem. J. 36, 191–195.
McDougall, I., Harrison, T.M., 1993. Geochronology and Thermochronology by the ^{40}Ar/^{39}Ar Method. Oxford University Press, New York. 269pp.
Morris, P.A., Kagami, H., 1989. Nd and Sr isotope systematics of Miocene to Holocene volcanic rocks from Southwest Japan: volcanism since the opening of Japan Sea. Earth Planet. Sci. Lett. 92, 335–346.
Nagao, K., Takahashi, E., 1993. Noble gases in the mantle wedge and lower crust: an inference from the isotopic analyses of xenoliths from Oki-Dogo and Ichinomegata. Japan. Geochem. J. 27, 229–240.
Nakamura, E., McCulloch, M.T., Campbel, I.H., 1990. Chemical geodynamics in a back arc region of Japan based on the trace element and Sr–Nd isotopic compositions. Tectonophysics 174, 207–233.
Niedermann, S., Eugster, O., 1992. Noble gases in lunar anorthositic rocks 60018 and 65315: acquisition of terrestrial krypton and xenon indicating an irreversible adsorption process. Geochim. Cosmochim. Acta 56, 493–509.
Nier, A.O., 1950. A redetermination of the relative abundances of the isotopes of carbon, nitrogen, oxygen, argon, and potassium. Phys. Rev. 77, 789–793.
Sano, Y., Nishio, Y., Gamo, T., Jambon, A., Marty, B., 1998. Noble gas and carbon isotopes in Mariana Trough basalt glasses. Appl. Geochem. 13, 441–449.
Scarsi, P., 2000. Fractional extraction of helium by crushing of olivine and clinopyroxene phenocrysts: effects on the ^{3}He/^{4}He measured ratio. Geochim. Cosmochim. Acta 64, 3751–3762.
Schmitt, A.K., Grove, M., Harrison, T.M., Lovera, O.M., Hulen, J., Walters, M., 2003. The Geysers–Cobb Mountain magma system, California (part 2): timescales of pluton emplacement and implications for its thermal history. Geochim. Cosmochim. Acta 67, 3443–3458.
Shaw, A.M., Hilton, D.R., Fischer, T.P., Walker, J.A., de Leeuw, G.A.M., 2006. Helium isotope variations in mineral separates from Costa Rica and Nicaragua: assessing crustal contributions, timescale variations and diffusion-related mechanisms. Chem. Geol. 230, 124–139.
Shiihara, M., Torii, M., Okuno, M., Nakamura, T., Kim, K.H., 2004. Correlation and AMS ^{14}C ages of tephra formation between U-2, U-3 and U-4 unit in the Ulleungdo, Korea and Oki 1 and 2 in the Japan Sea. Report on precise determination of volcanic eruption by ^{14}C wiggle-matching analysis of charred wood samples. Dating and Material Research Center, Nagoya University, Japan, pp. 74–89.
Shuto, K., Hirahara, Y., Ishimoto, H., Aoki, A., Jinbo, A., Goto, Y., 2004. Sr and Nd isotopic compositions of the magma source beneath north Hokkaido, Japan: composition with the back arc side in the NE Japan arc. J. Volcanol. Geotherm. Res. 134, 57–75.
Storey, M., Wolff, J.A., Morry, M.J., Marriner, G.F., 1989. Origin of hybrid lavas from Agua de Pau volcano, Sao Miguel, Azores. In: Saunders, A.D., Norry, M.J. (Eds.), Magmatism in the ocean basin. Geol. Soc. London, Special Pub., vol. 42, pp. 161–180.
Sumino, H., Nakai, S., Nagao, K., Notsu, K., 2000. High ^{3}He/^{4}He ratio in xenoliths from Takashima: evidence for plume type volcanism in southwestern Japan. Geophys. Res. Lett. 27, 1211–1214.
Sumino, H., Nagao, K., Notsu, K., 2001. Highly sensitive and precise measurement of helium isotopes using a mass spectrometer with double collector system. J. Mass Spectrom. Soc. Jpn. 49, 61–68.
Tamaki, K., 1988. Geological structure of Japan Sea and its tectonic implications. Bull. Geol. Surv. Japan 39, 269–365.
Tatsumoto, M., Nakamura, Y., 1991. DUPAL anomaly in the Sea of Japan: Pb, Nd, and Sr isotopic variations at the eastern Eurasian continental margin. Geochim. Cosmochim. Acta 55, 3697–3780.
Terakado, Y., Shimizu, H., Masuda, A., 1988. Nd and Sr isotopic variations in acidic rocks formed under a peculiar tectonic environment in Miocene Southwest Japan, Contrib. Mineral. Petrol. 99, 1–10.
Terakado, Y., Fujitani, T., Walker, R.J., 1997. Nd and Sr isotopic constraints on the origin of igneous rocks resulting from the opening of the Japan Sea, Southwestern Japan. Contrib. Mineral. Petrol. 129, 75–86.
Thirlwall, M.F., Jenkins, C., Vroon, P.C., Mattey, D.P., 1997. Crustal interaction during construction of oceanic islands: Pb–Sr–Nd–O isotope stratigraphy of the shield basalts of Gran Canaria. Chem. Geol. 135, 233–262.
Thompson, R.C., 1989. Structural stratigraphy and intrusive rocks at the Geysers geothermal field, Geothermal Resources Council. Transactions 13, 481–485.
van Soest, M.C., Hilton, D.R., Macpherson, C.G., Mattey, D.P., 2002. Resolving sediment subduction and crustal contamination in the Lesser Antilles island arc; a combined He–O–Sr isotope approach. J. Petrol. 43, 143–170.
Wasserburg, G.J., Jacobsen, S.B., DePaolo, D.J., McCulloch, M.T., Wen, J., 1981. Precise determinations of Sm/Nd ratios, Sm and Nd isotopic abundances in standard solutions. Geochim. Cosmochim. Acta 45, 2311–2323.
Yamamoto, J., Kaneoka, I., Nakai, S., Kagi, H., Prikhod'ko, V.S., Arai, S., 2004. Evidence for subduction-related components in the subcontinental mantle from low ^{3}He/^{4}He and ^{40}Ar/^{36}Ar ratio in mantle xenoliths from Far Eastern Russia. Chem. Geol. 207, 237–259.
Yokochi, R., Marty, B., Pik, R., Burnard, P., 2005. High ^{3}He/^{4}He ratios in peridotite xenoliths from SW Japan revisited: evidence for cosmogenic ^{3}He released by vacuum crushing. Geochem. Geophys. Geosyst. 6, Q01004. doi:10.1029/2004GC000836.
Zellmer, G.F., Annen, C., Charlier, B.L.A., George, R.M.M., Turner, S.P., Hawkesworth, C.J., 2005. Magma evolution and ascent at volcanic arcs: constraining petrogenetic processes through rates and chronologies. J. Volcanol. Geotherm. Res. 140, 171–191.
Zindler, A., Hart, S., 1986. Helium problematic primordial signals. Earth Planet. Sci. Lett. 79, 1–8.